AD-A040 953 UNITED TECHNOLOGIES RESEARCH CENTER EAST HARTFORD CONN F/G 11/4
FABRICATION AND EVALUATION OF LOW COST ALUMINA FIBER REINFORCED--ETC(U)
MAY 77 K M PREWO N00014-76-C-0035
UNCLASSIFIED UTRC/R77-912245-3 NL

1 OF 1
ADA040953

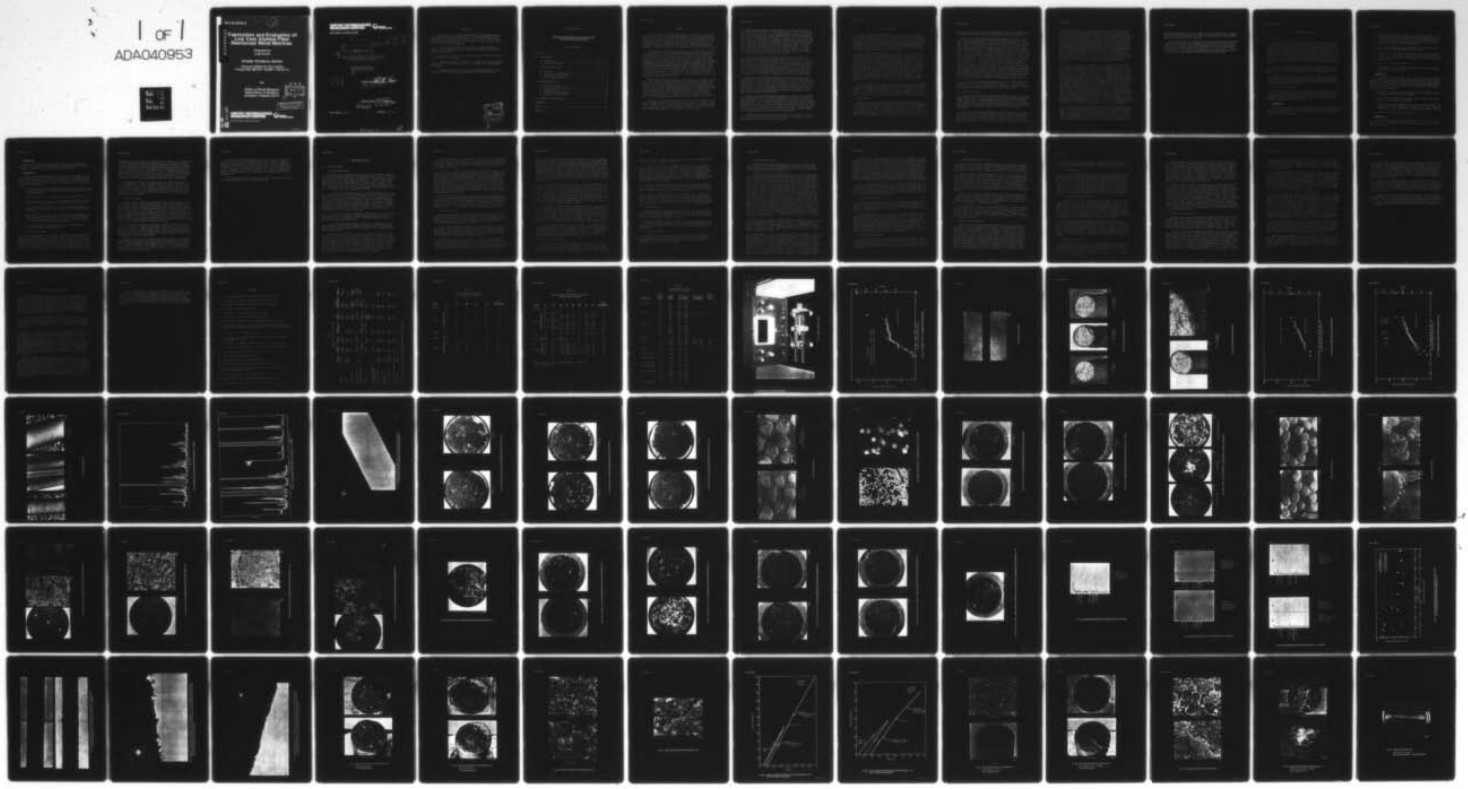

END

DATE FILMED
7-77

R77-912245-3

Fabrication and Evaluation of Low Cost Alumina Fiber Reinforced Metal Matrices

Prepared by
K.M. Prewo

INTERIM TECHNICAL REPORT

Contract N00014-76-C-0035
Project No. NR 031-784/9-1-76 (471)

for

Office of Naval Research
Department of the Navy
Arlington, Virginia 22217

UNITED TECHNOLOGIES
RESEARCH CENTER
EAST HARTFORD, CONNECTICUT 06108

UNITED TECHNOLOGIES

UNITED TECHNOLOGIES RESEARCH CENTER

UNITED TECHNOLOGIES

East Hartford, Connecticut 06108

(9) Interim technical rept. 1 Jul 75 - 1 Mar 77,

(14) UTRC Report R77-912245-3

(6) Fabrication and Evaluation of Low Cost Alumina Fiber Reinforced Metal Matrices.

Interim Technical Report
Contract N00014-76-C-0035

(15)

(12) 83 p.

REPORTED BY Karl M. Prewo

K. M. Prewo

(10) K a r l

APPROVED BY F. R. Thompson

F. R. Thompson, Manager
Materials Sciences

(11) DATE May 1977

NO. OF PAGES 78

COPY NO. _____

409252

(10)

ABSTRACT

This report describes the work conducted at United Technologies Research Center under ONR Contract N00014-76-C-0035. The contract monitor is Dr. B. MacDonald and the principal investigator is Dr. K. M. Prewo. The work described covers the period of July 1, 1975 to March 1, 1977. During this period the following have been accomplished.

1. Fiber properties important for achieving a strong composite were measured. These include axial fiber strength and strength distribution, and fiber surface chemistry.

2. Principles by which matrix composition should be chosen for successful infiltration were demonstrated.

3. Composite fabrication techniques were developed and refined to provide composites with excellent microstructures over a range of fiber reinforcement percentages.

4. Composite specimens for evaluation were produced and shown to exhibit high levels of mechanical properties predictable from fiber test data.

Report R77-912245-3

Fabrication and Evaluation of Low Cost Alumina Fiber Reinforced Metal Matrices

TABLE OF CONTENTS

SUMMARY

The herein described program was undertaken in an attempt to provide new directions for the field of metal matrix composites. In the past, metal matrix composite technology has concentrated on the use of expensive, relatively large diameter fibers and their incorporation into matrices through the use of hot pressing techniques. Although this has led to considerable success, major cost and process flexibility limitations have remained. Complex shapes are still difficult to fabricate and little or no use is made of metals casting technology.

This program recognizes recent developments in fiber technology which permit a reassessment of potential metal matrix composite systems. The fibers investigated to date on this program are all in multifilament yarn form and are highly flexible and easily handled. Cost projections for all of these fibers are competitive with graphite and well below the cost of large diameter monofilaments of boron and silicon carbide. The fibers are alumina fiber FP produced by DuPont Corp., a mixed oxide fiber AB 312 produced by 3M Corp., and a mixed oxide fiber, produced by Sumitomo Chemicals Corp. All composite matrices were aluminum alloys whose compositions were selected on the basis of melt surface tension and reactivity with the reinforcing fibers. The fabrication process chosen was vacuum infiltration casting. This process relies on the ability of the matrix to wet, and bond to, the fibers as it is being drawn into a mold containing a prealigned array of fibers.

Several significant accomplishments of this program can be readily identified. First, fiber properties important for achieving a strong composite were measured. These include axial fiber strength and strength distribution, and fiber surface chemistry. Second, principles by which matrix composition should be chosen for successful infiltration were demonstrated. Third, composite fabrication techniques were developed and refined to provide composites with excellent microstructures over a range of fiber reinforcement percentages. Fourth, composite specimens for evaluation were produced and shown to exhibit high levels of mechanical properties predictable from fiber test data.

The fibers tested exhibited marked differences in surface chemistry, surface topography, mechanical properties and fracture modes. Individual filament tensile strengths of up to nearly 4000 MPa were measured with average strengths of up to 2000 MPa. These high strengths are noteworthy because of the low cost mass production procedures used to produce all of these fibers.

Aluminum alloy matrices containing significant alloying additions of Li, Bi and Mg either individually or in combination were all shown to infiltrate fiber filled molds. In each case the alloying additions lowered the melt surface tension sufficiently to achieve infiltration while pure molten aluminum, even at very high temperatures, was unable to penetrate the fiber arrays. Although several elements were thus available, alloying systems based on the use of at least some Li provided the best bond to the fibers and also infiltrated fiber arrays most completely on both the micro and macro scales. This was associated with reaction between the Li and the fiber surfaces. By using an alloy containing both Li and Mg as well as a small addition of Zr, it was possible to fabricate composites based on the FP alumina fiber with a matrix whose mechanical properties should also be excellent.

Composite fabrication procedures included the use of both fluxed melt surfaces and melting under argon, and also a comparison between the use of preevacuated fiber filled molds and molds containing fibers and air. Composite fabrication by pressurization of the melt surface, forcing molten alloy up into a fiber filled mold was demonstrated to be a viable technique as was the more conventional use of a vacuum to pull metal into the mold. It was concluded that, in the case of a properly chosen fiber-matrix combination, all of these processes were usable and that this considerable flexibility of fabrication procedure would be of significant advantage in possible future applications.

Composites with axial tensile strengths of up to 620 MPa were produced through the use of the FP alumina fiber. Analysis of stress-strain curves indicated, as in the case of other metal matrix composites, that a bilinear stress-strain curve is characteristic of material behavior. The initial linear portion coincides with the elastic deformation of both fibers and matrix while the secondary linear portion is characteristic of elastic fiber and plastic matrix deformation. Both composite strengths and elastic moduli agreed with predictions based on measured fiber properties.

Because of these excellent mechanical properties and the relatively simple casting techniques usable for article fabrication, these composite systems are being considered for use in engineering applications. Although specific mechanical properties (property divided by density) are not superior to boron reinforced aluminum composites, the combination of properties with anticipated low cost can open up new areas of application not previously considered. The selective stiffening of gear box housings and gas turbine engine vanes are just two examples under consideration within United Technologies Corporation.

This program is being continued with the purpose of expanding the range of fiber and matrix combinations and also performing greater in-depth evaluation of mechanical properties and environmental stability.

I. INTRODUCTION

Continuous filament reinforced metal matrix composites are slowly, but surely, finding their way into areas of application and component production. This progress has been much slower for these systems than for their counterpart resin matrix composites because of cost, fabrication and, in some cases, performance penalties. At last, however, boron reinforced aluminum components are being produced and sold in both the aerospace and consumer areas. Although still a very modest beginning, it is now foreseeable that other less well developed metal matrix systems will also come into use.

Small diameter oxide fibers were one of the first choices seriously considered and evaluated as reinforcements for metal matrix composites. Both in the United States and England a number of programs were directed at utilizing silica and other glass type fibers. The work of Morely, Cratchley and Baker in England (Refs. 1-5) was probably the most successful in this area, however, other programs in the United States were also attempted (Refs. 6,7). In each case silica base fibers of extremely high strength were coated with aluminum to achieve an aluminum matrix composite. The process was usually performed in a series of steps and in each case considerable care was taken to minimize chemical and mechanical degradation of the reinforcing fibers which were on the order of 20μ in diameter. The considerable difficulty in fabricating these composites and their resultant low modulus and moderate strength, as compared to boron reinforced aluminum, prevented these systems from receiving wider acceptance.

More recently the use of graphite yarn has been explored as a reinforcement for metals. The greatest success has been achieved with aluminum alloy matrices, however, nickel, magnesium, copper, zinc, lead and even beryllium have all been attempted. The magnitude of effort and large number of programs to achieve a graphite yarn reinforced aluminum has been truly impressive, and it can now be said that composites with high axial tensile strength can be fabricated (Ref. 8).

A. Alumina Fibers

In the past two years several very attractive alumina type yarns have become available in experimental quantities. These fibers offer the possibility of high specific properties, low cost, environmental stability and compatibility with aluminum alloys. This combination of fiber qualities clearly points to significant potential for the alumina reinforced aluminum system. Although composite mechanical properties at room temperature will be less than those characteristic of boron aluminum, the low fiber cost, extreme ease of composite

fabrication, and resultant composite environmental stability all indicate that this system could open new areas for metal matrix composite application.

Alumina fiber has been available for several years. It has been of particular interest for application in metal matrix composites because of its excellent strength and modulus, particularly at high temperature. The two principal examples of alumina fiber to be utilized in the past are large diameter (>250μ) single crystal rods, manufactured by the Tyco and A. D. Little Laboratories, and alumina whiskers. The large diameter rods, unfortunately, suffer from a series of problems which include: extreme sensitivity to handling and surface defects, a tendency to twin during compression loading in the metal matrix on cooling after fabrication, and reactivity with nickel base alloys. The greatest impediment to their use, however, is their extreme high cost which, at present, is approximately $2 per foot and shows little possibility of ever being very inexpensive. Alumina whiskers also have been given considerable attention; however, in this case all efforts have also failed because of the extremes of difficulty in fabrication, high cost of good quality whiskers and resultant low composite strength. In these cases of previous work, alumina had been considered for titanium and nickel base alloy reinforcement and relatively high temperature (500-1100°C) application. No concerted effort was made to use alumina fibers in aluminum alloys because it was clear that boron fibers would produce far superior and less expensive composites which, because of matrix limitations, would only be considered for application up to about 350°C.

The current investigation utilizes fibers of alumina and also mixed oxides to explore the potential for high performance composites. These fibers are available from E. I. DuPont de Nemours & Co., 3M Company, and Sumitomo Chemicals Ltd. Each will be discussed in detail in the body of this report.

B. Fabrication and Matrix

Composite fabrication with alumina yarn must emphasize the use of casting and liquid infiltration techniques. Ample experience with carbon yarn and small diameter glass fibers has demonstrated that the hot pressing of unprotected small diameter fibers can lead to large scale fiber breakage. This casting requirement is not a limitation of extreme concern, however, since it is precisely this ability to cast composites which is needed in metal matrix composite technology.

The choice of fiber-matrix combination is critical to the success of any infiltration procedure. The matrix must be compatible with the fiber, a good casting alloy, and a good matrix in terms of its environmental and mechanical properties. The first two criteria assure the fabricability of the composite while the last determines, to a large part, the utility of the resultant composite.

Recent work, performed at the Pioneering Research Division of E. I. DuPont de Nemours Co., has demonstrated that aluminum alloys containing several percent lithium satisfy the first, and at least in part, the second and third of the above-mentioned criteria when used in conjunction with DuPont's FP alumina fiber, (Ref. 9). Preliminary experiments at United Technologies Research Center, prior to this program, confirmed the ease with which this fiber-matrix pair could be combined by liquid metal infiltration. Additional data in the literature, however, indicate that the aluminum-lithium binary alloy can be improved upon to achieve superior mechanical properties, environmental stability, and enhanced ease of castability. Emphasis has been placed on the use of major additions of Cu and Mg to increase the response of the system to heat treatment (Refs. 10-13) while the use of trace elements of Cr, Mn, Zr and others has been explored to achieve microstructural refinement and also affect heat treatment (Refs. 10,13). The use of small additions of Ti, Zr, B, Be and Si has also been shown to improve the oxidation resistance of the melt and the resultant metal alloy (Ref. 14).

Besides lithium, the other primary elemental additions considered during this program were magnesium and bismuth. Both of these elements, along with lithium, are very effective melt surface tension depressants (Ref. 15). Bismuth and lithium exhibit almost an identical ability to lower aluminum alloy surface tension in argon. The addition of 2% by weight of either element causes a 40% decrease in melt surface tension at 700-740°C. The addition of 6% magnesium is less effective and causes a depression of 30% at the same temperature. Depression of the metal surface tension is an effective way of improving the fabricability of a fiber-matrix combination. This was illustrated by the work of Sutton who calculated the magnitude of external pressure required to cause the infiltration of liquid nickel into the channels between alumina fibers (Refs. 16,17). He found that the required infiltration pressure increased with increasing volume fraction fiber, increasing metal surface tension and was inversely proportional to fiber diameter. Although infiltration in a nonwetting system such as Sutton's could be achieved through the application of external pressure, upon cooling of the composite, voids and areas of fiber-matrix disbond were created due to the fact that the matrix did not wet the fibers. It can also be shown, using Sutton's calculation, that many small pores and voids would remain in any realistic fiber array due to the existence of crossovers and regions of nonuniform packing.

In a system in which the matrix wets the fibers, however, limited infiltration can occur spontaneously without the need for the application of external pressure. Wetting, however, must not be achieved at the expense of overreaction between fiber and matrix. Both magnesium and bismuth additions to aluminum can cause, through reaction, at least some wetting of alumina and glass fiber surfaces. It was bismuth that was used as the elemental addition to aluminum to control reaction with silica fibers in the first attempts to fabricate silica

reinforced aluminum (Ref. 18). The addition of up to 4.5% magnesium to aluminum alloys has also been demonstrated to permit the incorporation of alpha alumina particles into the molten alloy (Ref. 19).

One additional point to be noted is that recent experiments on NASA's SKYLAB flights have demonstrated the importance of melt agitation to achieve wetting (Ref. 20). It was shown that, by rapid agitation of the melt, it was possible to achieve well bonded composites of Al-Al_2O_3, Al-SiC, Al-C and Al-W. It was the contention of the authors of this work that, by removal of any occluded gases from the solid-liquid aluminum interface, wetting could be promoted.

II. EXPERIMENTAL PROCEDURES

A. Materials

The fibers chosen for this program consist of three commercially available continuous yarns and one experimental fiber that was available only in limited quantity. Fiber property data, available from the manufacturers, are presented in Table I and compared with data for boron, and single crystal alumina. The DuPont FP fiber was procured in both the Type I and Type IV forms. Both of these are available in continuous tows containing approximately 200 fibers each. The Type I fiber is pure alpha alumina while the Type IV is coated with a thin layer of silica. The AB 312 fiber is also a continuous tow; however, it is not pure alumina but instead a mixed oxide of alumina, boria and silica. It was supplied with an organic surface coating which was intended to protect the fiber during handling.

The only fiber not available in large quantity continuous length was a mixed oxide of alumina and silica made by Sumitomo Chemicals Ltd. This fiber was available in tow form of several meters length with approximately 50 fibers per tow.

All of the matrices were aluminum alloys. One aluminum alloy containing 5% lithium was purchased from the Belmont Melting and Refining Works, Brooklyn, New York, while all other alloys were made by inert atmosphere melting practice at UTRC from elemental starting components.

B. Composite Casting Procedures

Five different procedures were used to fabricate composite specimens. All of these involved the infiltration of prealigned arrays of fibers with molten aluminum alloys. In every case 10 cm lengths of fibers were held within one end of 30 cm long 0.45 cm internal diameter stainless steel tubes. The five procedural variations are discussed below.

Procedure (1)

In this case the stainless steel tube containing the fibers was open at both ends. The molten aluminum alloy to be used for infiltration was held under a flux in a crucible heated in air. Once the melt was at the desired temperature the following steps were carried out.

1. Submerge one end of the tube beneath the surface of the melt. The tube is submerged to a depth which permits the entire length of fiber to be beneath the melt surface. Note that at this stage molten metal does not infiltrate up into the fibers and they are essentially in an air atmosphere at the surrounding melt temperature.

2. The tube-fiber assembly is held in the melt for a desired length of time to insure appropriate preheat of the fibers.

3. A vacuum line is connected to the free end of the tube and a vacuum applied. At this time molten metal is drawn up between the fibers and continues up the tube until it solidifies at some point above the melt surface level.

4. The tube is removed from the melt.

5. The resultant rod of composite is then removed from its steel jacket by grinding away the outer tube.

Procedure (2)

This procedure differs from number (1) in that the one end of the stainless steel tube nearest the fibers was sealed with a 50μ thick stainless steel diaphragm. This welded closure was vacuum tight so that a vacuum of approximately 20 microns could be achieved by the connection of a mechanical vacuum pump and vacuum gauge to the open end of the tube. Once this vacuum had been achieved the following steps were taken.

1. Submerge the sealed end of the tube beneath the molten metal surface to a depth that covered the fiber length.

2. Hold the tube in the melt for a desired length of time to preheat the fibers in their evacuated environment.

3. Rupture the steel diaphragm while still beneath the melt surface. This caused molten metal to be pulled up, surrounding the fibers. This was accompanied by a brief partial loss of vacuum as measured by the gauge.

4. Remove the infiltrated tube from the melt.

Procedure (3)

The only difference between procedures (3) and (2) is that in this case the melt was held in a closed chamber under an argon atmosphere, thus eliminating the need for a flux.

Procedure (4)

This procedure is identical to procedure (3) except that a vibrator was attached to the steel tube and operated during alloy infiltration. The vibrator was coupled mechanically to the tube at a level above the melt.

Procedure (5)

Unlike all of the above procedures, in this case the molten metal was essentially "pushed" up around the fibers rather than "pulled". The molten alloy was held in a closed chamber under argon and the stainless steel tube was once again sealed at one end, however, in this case the end sealed was the one opposite that in which the fiber was held.

1. The open end of the fiber containing tube was introduced into the chamber through a vacuum tight sliding seal, however the tube was not put in contact with the melt.

2. Both the chamber and tube are pumped down to a vacuum of 10^{-5} torr.

3. The open end of the tube (the end which contains the fibers) is lowered beneath the surface of the melt to a depth which covers the fibers.

4. The tube is held in this position, with the vacuum maintained over the melt, for a desired preheat time. The fibers are thus being preheated in vacuum.

5. Argon is bled back into the chamber to finally achieve atmospheric pressure. Because the open end of the tube is beneath the melt surface, and because the inside of the tube is still at 10^{-5} torr, molten metal is forced up into the tube and around the fibers.

6. The infiltrated tube is then removed from the chamber which now is filled with argon at atmospheric pressure.

C. Mechanical Test Procedures

The as-received fibers were tensile tested to determine fiber strength distribution. The fiber tensile test apparatus is shown in Fig. 1. The test procedure consists of mounting individual fibers between the arms of the apparatus and then securing the fiber ends with a droplet of hot wax at each end. A tensile load is then applied by turning the dial-screw mechanism and the load applied to the fiber is measured by a system of calibrated strain gages bonded to one of the test arms. The load at failure is recorded for each fiber. After test the

remaining fiber halves are used to measure the fiber diameter in the gage section by use of an optical microscope and calibrated eyepiece. To aid in observing the mode of fiber fracture, selected fiber specimens are submerged in a droplet of water supported by a small stage placed directly beneath the fiber gage section. This droplet acts as a containment for the fiber fragmentation process during fiber failure and as a result it is possible to determine where the fiber fractured and in how many locations it fractured. Examination of fiber fracture surfaces by scanning electron microscopy is then performed on selected fiber fragments, or more usually, on fibers which fractured in only one location.

The infiltrated composite specimens were tensile tested in the form of 0.38 cm diameter rods. These were removed from the stainless steel tubes, used for infiltration, by centerless grinding. Hollow cylindrical steel grips were epoxied onto each specimen end. These were threaded on the outside to fit into the tensile test machine. The specimen gage length was 2.54 cm and two strain gages were attached to opposing sides of the gage section when stress-strain response was to be measured.

D. Fiber Surface Analysis

Analysis of fiber surface chemistry was performed on fibers in both the as-received and extracted (from composite) states. The principal technique used was Secondary Ion Mass Spectrometry (SIMS) using a 3M model 52B unit. This unit is capable of both Ion Scattering Spectrometry (ISS) and SIMS. In ISS a primary beam of ions is directed at the surface to be studied at low fixed energies. The scattered ions, originating from the primary beam, are analyzed in an electrostatic energy analyzer and, by this analysis, used to identify the elements on the specimen surface. It is found also, however, that atoms and compounds can be removed from the specimen surface by this process and the analysis of these secondary ions with a mass spectrometer forms the basis for SIMS.

In SIMS, chemical information about surface composition (~5Å information depth) of a sample is obtained by sputtering the sample with a 1.5 to 2.0 mm diameter beam of ions [here $(Ne^{20})^+$ at 1500 volts]. Ions sputtered from the surface are passed through a UTI 300C quadrupole mass spectrometer which is preceded by an energy filter to reject ions with energies greater than about 100 volts. Both conductors and insulators can be studied.

The SIMS signal output is a readout of detected ion current vs mass number. Sputtered ions can be both elements and fragments of compounds, and the distribution of compound fragments (cracking pattern) can serve to identify compounds on the surface by comparison with standards. Shallow (less than 1000Å) depth profiling can be done by sputtering into the surface and sampling the SIMS spectrum after various sputtering times.

The probability of detecting a particular species depends not only on its abundance but also on the sputtering probability and the ease of ionizing it during the sputtering process. The latter two factors are host or substrate dependent as well as species dependent. Thus, while a particular peak height may be proportional to the amount of that species present in the sample, quantitative comparisons can only be made between similar samples, and absolute abundance can be determined only by comparing with a known standard of similar characteristics.

Electron diffraction analysis was also performed on selected fibers to provide a more complete analysis of surface composition.

III. EXPERIMENTAL RESULTS

A. As Received Fibers

1. Mechanical Properties

The tensile test data obtained by testing individual filaments of DuPont's fiber FP-IV are presented in Fig. 2. The gage length was 0.63 cm (0.25 in.) and three distinct strength populations were observed. The lowest strength fibers were all found to be somewhat kinked or curved prior to test while the fibers populating the middle strength range were visually straight. Figure 3 illustrates the type of kinks observed in the fibers. Finally, two specimens out of the set were observed to exhibit very high strengths. The significance of each of these strength regimes is considered in turn below.

a. The lowest strength population is not characteristic of the FP material itself, but instead is due to the kinked condition. In testing an elastic prestress is induced on the surface of the fiber as it is straightened. The areas of the fiber in which this prestress is tensile then fail at a lower observed UTS than characteristic of the material itself. The radii of curvature of the kinks observed could cause stresses in excess of 2000 MPa to be superimposed onto the average tensile stresses during fiber tensile test. The actual superimposed bending stress is probably considerably less, however, due to straightening of the fiber prior to fracture.

b. The highest levels of strength are indicative of the strength potential for this fiber. Observation of these levels should encourage further investigation into the fundamental strength controlling mechanisms of this polycrystalline alumina fibrous structure.

c. The middle strength range is typical of the predominant flaw population, probably relatable to the material structure, which is different from the visual kinks discussed above, yet which also lowers fiber strength from the highest levels observed.

The average tensile strength of all of the FP fibers tested was 1760 MPa (255×10^3 psi) while that of only those fibers which did not exhibit the large scale kinks is 2040 MPa (288×10^3 psi). At present it is unclear as to which of these numbers would be more influential in determining resultant metal matrix composite strength. In addition it should be noted that, although the values of strength reported are not, on the average, extremely high, they are strengths measured after handling of the fiber. In the past, alumina monofilaments have been available with higher "as received" strength, however, in every case handling and slight abrasion caused major reductions in strength.

The fracture surfaces of FP fibers appear to be similar to the outer fiber surface, i.e., granular, Figs. 4 and 5. It was not possible to correlate fracture surface appearance with measured tensile strength. In addition, because of the granular surface, it was not possible to clearly define the locations of fiber fracture initiation.

Fiber AB-312 is a mixed oxide ceramic fiber produced by 3M Company. It is available as a continuous yarn with 390 filaments per tow. It is primarily designed for use as a high temperature material in heat shields and thermal insulation, however, the manufacturer indicates a higher strength reinforcing grade of fiber is possible in the future. The strength distribution of fiber AB-312 is given in Fig. 6. There was no observable evidence of fiber kinking and the normal distribution of fiber strength indicates that all of the fibers tested failed due to one controlling type of flaw population. The highest strengths observed were approximately 2000 MPa which is well below the highest values of the FP fiber, however, the lower density of AB-312 provides a specific strength advantage for this fiber.

The Sumitomo Chemicals fiber is a yarn consisting of alumina and silica. The silica helps stabilize the alumina against grain growth at elevated temperatures so that this fiber has high temperature stability. Two small samples of this fiber were delivered to the Research Center for evaluation and both were evaluated by tensile test. The data obtained for both deliveries of fiber are presented in Fig. 7. As in the case of AB-312, kinking was not observed.

2. Surface Condition

The surface structures of the fibers are compared in Fig. 8. The FP fiber surface is very rough and irregular as compared to the very glassy smooth surfaces of the other two fibers. Both the FP-I and FP-IV fibers exhibit the same rough surface characteristics with no discernible difference attributable to the thin coating of SiO_2 present on the latter.

Figure 9 shows the SIMS mass spectrum for FP-I fibers taken at an approximate depth of 50Å. The spectrum changed somewhat with time during the early sputtering, but stabilized to that shown in Fig. 9 by the time 20 to 30Å had been sputtered away. Spectra for the other fiber types were somewhat similar to this, and thus this one will be discussed in detail.

The peaks at mass 10 and 20 are doubly ionized and singly ionized Ne^{20} respectively - the probe gas. Lines at mass 1, 23, and 39 are H, Na, and K which were present in all of the samples. These elements are seen often in SIMS spectra, but they usually decay away after a moderate amount of sputtering while here they persisted well into the fibers. The collection of lines at 12, 13,

14, 15, 16 is a typical cracking pattern from an organic. These are probably C, CH, CH_2, CH_3, CH_4. Lines at 41 to 45, 57 to 59, and 76 also probably come from organic residues and probably indicate a fairly heavy polymer. Some contributions to the lines at 27 and 28 likely come from Al^+ and AlH^+ with the rest also coming from organics. The other lines from 26 through 31 are likely of organic origin. While we don't know the precise contribution to 27 and 28 from Al, AlH, and Si, the peak height ratio for mass 27 to 28 stabilized at 1.85 after about 20Å of sputtering and can be considered to be characteristic of FP-I fibers. For reference, the relative instrument gain for the H peak is 1 while the gain is 10 for the rest of the spectrum. The lines at 63 and 65 are Cu from the sample mount.

Data for FP-IV fibers are shown in Fig. 10. Figure 10A corresponds to a depth of about 5Å (gain 1 for H, 10 for the rest), and Fig. 10B is for a depth of 75Å at a gain of 2.5. These fibers are supposed to have a thin coating of SiO_2 on the surface, and the peak height ratio of 27 to 28 at 5Å of 0.74 compared with the above 1.85 is clearly consistent with the presence of Si^{28}. At a 75Å depth, the 27 to 28 ratio is 1.75 - close to that for FP-I fibers. This latter ratio had stabilized at about 50Å which thus represents an average thickness for the SiO_2 film. One other difference to note in Fig. 10B is that the peaks from organics are greatly decreased over those in 10A and in contrast to FP-I fibers which still showed organics at 100Å.

Both the AB-312 fibers and the Sumitomo fibers exhibited some organics on the surface but organic peaks decreased by a factor of 3 or so after only about 20Å of sputtering. It should be noted that the AB-312 fiber was heat treated in air prior to examination to remove a protective organic sizing used by the fabricator. The organic peaks in these two fibers (relative to Al) were about 10 times smaller than in the FP-I and FP-IV fibers. The mass 27 to 28 ratios are 5.2 and 1.8 for AB-312 and Sumitomo respectively. AB-312 fibers showed the presence of some Li, and a trace of Li was also found in the Sumitomo fibers.

To provide additional analysis of the FP-IV fiber, electron diffraction patterns were obtained at the fiber surface. The resultant pattern, shown in Fig. 11 with a profile view of the fiber, was spotty due to the small number of microstructural grains in the diffracting field. Attempts at indexing the pattern, however, showed possible agreement with three SiO_2 compounds. The best match was with hexagonal SiO_2 (ASTM Card No. 12-708).

B. Composite Casting Procedures

All of the composite casting procedures described in section II-B were found capable of producing infiltrated composites. Resultant composite microstructure was much more sensitive to the matrix alloy composition and temperature of infiltration used, than to variations within the casting procedural types.

Several observations, however, clearly indicated desirable aspects of procedures 2, 3 and 4. These are summarized below.

1. The use of a thin steel diaphragm on the end of the fiber filled tube proved desirable in the case of both flux covered (air melting) or unfluxed (melting under argon) molten alloys. The diaphragm permitted complete preevacuation of the fiber filled preform prior to infiltration of the molten alloy. This minimized the occurrence of voids in the resultant microstructure which previously had resulted from entrapped gas. In addition, the diaphragm prevented the entrapment of melt surface dross in the open end of the tube as it was lowered beneath the melt surface.

2. The use of an argon cover gas negated the requirement for a flux and thus improved the purity and cleanliness of the melt. In addition, the loss of Bi, Li and Mg due to reaction at the melt surface in air, and the volatilization of these elements from the melt in vacuum, was prevented.

3. The use of a vibrator was not clearly demonstrated to be beneficial. In the experiments performed the mode of vibration set up was a flexural wave down the steel tube. Thus, because of the wave form, the amplitude of vibration varied with position. Therefore, the degree of infiltration varied with location along the tube and it could not clearly be stated that infiltration was aided.

C. Alloy Composition

Alloy composition and melt temperature were the two most critical factors in controlling composite infiltration. Each of the alloy systems investigated will be discussed below and summaries of extracted fiber and composite property data will be presented in the next two sections.

Table II is a compilation of the compositions of the starting alloys prior to infiltration. These data are based on the weighed elemental additions made to form each alloy while the data in Table III are from chemical analyses of the actual melts.

1. Unalloyed Aluminum

Infiltrations were performed with tubes containing 50% by volume of FP-I, FP-IV and AB-312 (precleaned) fibers using procedures 4 and 5. Infiltration temperatures of as high as 840°C were tried and, in every case, absolutely no infiltration of the fiber bundles occurred.

2. Aluminum-Lithium Alloys

As was anticipated, numerous experiments with lithium containing alloys were successful in providing a fully infiltrated structure. All of the procedures described were tried and each was successful for specific combinations of fiber, matrix composition and temperature.

In the simplest case (Melt designated #1, Tables II,III), infiltrations were successfully performed using process number one and the aluminum-lithium (4% Li) alloy purchased from Belmont metals. Using fiber FP-IV, the effects of preheat hold time, melt temperature, post infiltration hold time and volume percent fiber were all examined. Of these, melt temperature and volume percent fiber were most important. Specimens 1-22 and 1-23, Fig. 12, indicate that fairly high void contents were obtained at 700°C while at 720°C somewhat fewer voids were noticeable. Other attempted specimens which were infiltrated at 670°C proved totally unsatisfactory with very little metal infiltrating the fiber bundles at all. The specimens shown in Fig. 12 contained approximately 50% fiber by volume. The specimens in Figs. 13 and 14, however, contain varied percentages of fiber. It was found that the number of distributed voids and poorly infiltrated areas decreased with increasing volume percent fiber. The effect of pre and post infiltration hold times was not found to be very significant from a microstructural point of view. High magnification examination of specimens held in molten alloy for 15 seconds (spec 1-10) and 60 seconds (spec 1-12), Fig. 15, did not indicate any difference in fiber-matrix interface. In both cases molten metal was able to penetrate even the smallest of fiber-fiber spacings. Overreacted fibers could be detected optically, however, when longer hold times were used, Fig. 16. The rough surface of the FP fibers is clearly discernible in both cases.

The use of the preevacuation technique, procedure number two, caused a considerable improvement in composite microstructure. The structures shown in Fig. 17 were obtained using the preevacuation step and can be compared with Figs. 12-15. The void content, both distributed between the fibers and at the mold-composite interface decreased to almost zero, particularly in the case of the composite containing 50% fiber.

The percentage of Li present in the melt was extremely important. Excellent microstructures were obtained with Li contents in excess of 2% and even at 1.6% it was possible to achieve nearly complete infiltration, Fig. 18. However, this was at the approximate limit for reproducible results. At a level of 1.2% Li the composite structure varied with location in the infiltrated tube. The microstructures shown in Fig. 19 are all from the same composite, however, at different locations. At the end of the composite which first reacted with the Al-1.2% Li alloy, infiltration was nearly complete. At composite sections further removed from this end the degree of infiltration became less and less complete, apparently due to a depleted supply of Li in the melt because of reaction with the fiber.

It was found that large percentages of iron were being picked up during the infiltration process. In the cases where the Belmont alloy was used, the initial starting material contained 0.5% iron and this was a major source of iron for infiltrations 1 through 7 and 19. It was not the sole source of iron, however, because levels were reached in excess of 1%, and in the case of specimens made from melt 7, the microstructure contained observable $FeAl_3$ particles. Iron pick-up during infiltration was occurring by reaction with the steel mold tubes and with a stainless steel thermocouple sheath used to protect a submerged thermocouple. When alloy compositions were made at UTRC using our own high purity starting elements, the iron content could usually be held to less than 1% unless a very large number of composite infiltrations, over a very long time, were made.

All infiltrations performed with both fibers FP-I and AB-312 were much less successful. Selective infiltration would occur in localized areas, however, the overall microstructures contained large numbers of voids. The matrix would tend to channel up around groups of fibers, rather than surround each individual fiber. When intimate contact did occur, the AB-312 fibers appeared to react excessively with the lithium bearing matrix, Figs. 20,21.

3. Aluminum-Bismuth Alloy

Infiltrations performed with bismuth as the only alloying addition to aluminum were less successful than those described above for alloys containing lithium. Although the intended alloy composition was 2% Bi, the actual melt used in these experiments contained only 1.4% Bi due to loss during vacuum melting prior to infiltration.

It was generally possible to infiltrate all three fiber types, FP-IV, FP-I and AB-312; however, not without the presence of some voids. The FP-IV fiber reinforced composite structure shown in Fig. 22 was a typical result. A large amount of fiber "bunching" took place and the matrix was not always able to separate the fibers and penetrate between them. Intimate contact and good fiber-matrix distribution was achieved, however, in some local areas, Fig. 22c. Figure 23 demonstrates the same sort of structural features where fiber FP-I was used, and Fig. 24 for fiber AB-312. The Al-Bi alloy appeared to react less severely with the AB-312 fiber than did the Al-Li alloys.

4. Aluminum-Magnesium Alloys

As in the case of bismuth containing alloys, magnesium additions to the melt permitted macro scale infiltration to take place, however, the composite microstructure contained many voids and areas of bunched together fibers. Alloys containing 10% and 12% magnesium were used and typical microstructures are shown in Figs. 25 and 26.

5. Aluminum-Magnesium-Lithium Alloys

Alloys containing these two primary elemental additions, and in one case a small amount of zirconium, were successfully used to infiltrate composites when the levels of alloying were high enough. It was demonstrated that low levels of lithium can be used provided the magnesium concentration is raised appropriately.

Referring to Table III, alloys containing as low as 0.4-0.5% Li were successfully used to infiltrate FP-IV fiber composites. The structure obtained by use of an alloy containing 0.4% Li and 10.4% Mg is shown in Fig. 27. This is comparable to the levels of infiltration possible using lithium concentrations above 1.2% without magnesium. If the level of magnesium is dropped significantly, however, the degree of infiltration also diminishes. The microstructures in Fig. 28 were obtained using an alloy containing 0.5% Li and 5.3% Mg. The amounts of fiber bunching and porosity increased significantly with the decrease in magnesium content.

Higher levels of lithium and magnesium resulted in additional improvements in overall composite microstructure, Fig. 29, although when the percentage of Li remained below 1.2% it was not possible to get completely void-free composites. It was also shown that the addition of a small percentage of zirconium to the melt was not detrimental to infiltration, Fig. 30.

Another experiment tried with the Al-Li-Mg-Zr alloy was to include aluminum wires in with the FP-IV fiber array. In this way it would be possible to demonstrate a capability to selectively reinforce a structure and also provide an alternate means for achieving low fiber content composites. Although the resultant composite microstructures were not void free, a reasonable level of infiltration was achieved, Fig. 31.

D. Analysis of Extracted Fibers

FP-IV fibers were extracted from infiltrated composites by dissolution of the matrix. This was performed in such a way as to permit an analysis of the chemistry of the extracted matrix to be performed. A comparison was made with the composition of the parent alloy. It was generally found, but not always, that the matrix lithium content was several tenths of a percent below that of the parent alloy. Also, it appeared that bismuth and magnesium percentages were unchanged when comparisons between parent alloy and composite matrix were made. This limited indication of reaction between fiber and matrix, when lithium is present in the melt, was confirmed by the visual appearance of the extracted fibers. Those extracted from matrices containing high percentages of lithium were dark grey in appearance while those taken from alloys containing only bismuth or only magnesium were as white in appearance as the as-purchased fiber.

Several of the sets of FP-IV fibers that were removed from the infiltrated composites were analyzed using secondary ion mass spectroscopy. The results of this type of analysis are discussed below for four different alloy matrices.

1. Aluminum-Bismuth

As was described above, the color of FP-IV fibers extracted from an aluminum-bismuth alloy composite was unchanged from that of the original FP fibers. The SIMS mass spectrum for the fibers extracted from FP-IV/Al-Bi composite 9-21 is shown in Fig. 32. The spectrum shown only covers 0-40 atomic mass units, however, an examination of the higher atomic mass spectrum for Bi (209) revealed a complete absence of this element from the fiber surface. Only Al and Si, with slight traces of Li and Na, were detected. The ratio of Al to Si peak heights is about 4.0 which is much higher than a similar ratio of 0.74 for as-received FP-IV fiber. Thus, it appears that, although no substantial reaction has taken place, the SiO_2 coating was removed from the fibers by the infiltration process.

2. Aluminum-Magnesium-Lithium Alloys

The aluminum 0.5% lithium - 5.3% magnesium alloy matrix did not alter the visual appearance of FP-IV fiber significantly and the SIMS spectrum, Fig. 33, indicates only a slight presence of Mg on the fiber surface. The ratio of aluminum to silicon peak heights for the fibers extracted from composite 15-1 is about 5.0 which, as in the case of the Al-Bi alloy above, indicates the removal of most of the SiO_2 from the fiber surface. It is interesting to note that some Li was present on the fiber surface. Although the ratio of aluminum to lithium peak heights is 0.9, the actual surface concentration can still be very dilute in Li, because Li is easily removed from the surface during sputtering.

The aluminum-magnesium-lithium alloys containing higher percentages of lithium, however, did cause a noticeable visual change in fiber color and this can be associated with the reaction of Li with the fiber surface. The SIMS spectrum for fibers extracted from specimen 18-1 (1.7% Li, 4.0% Mg) is shown in Fig. 33. A very high rate of removal of Li atoms is evident, which agrees with the change in fiber surface color. In addition the ratio of aluminum to silicon peak heights is very high indicating nearly complete removal of any SiO_2 from the surface.

3. Aluminum-Lithium Alloys

The presence of lithium in the melt definitely caused a major color change in the fiber surface. This change is associated with reaction of the Li with the FP-IV fiber, and as shown in Fig. 34 for specimen 6-15, the presence of significant amounts of Li on the fiber surface. The contrast between fibers extracted from two alloys containing 1.7% Li is also shown in Fig. 34. Specimen 18-1 also contained 4% magnesium.

The sputtering of the fibers extracted from composite 6-15 was continued for up to 200 minutes to determine the depth of reaction layer of Li within the fiber. Depth measurements are very approximate; however, the data in Fig. 35 are presented to give a general appreciation for the reacted layer thickness. The peak height ratio of Li to Al dropped off rapidly with sputtering time so that after about 100 minutes (or 42Å based on the sputtering rate of Al_2O_3) a stable ratio of 7.5 was achieved. Similarly, the ratio of Al to Si peak heights stabilized at about the same value at the same sputtered depth. Lithium is clearly present in significant concentrations at considerably greater depths, however, no additional sputtering was carried out.

Electron diffraction analysis was performed on FP-IV fibers extracted from Al-1.7%Li matrix composite 6-15 in an attempt to establish the nature of the reacted fiber surface. A comparison between as-received and chemically extracted fibers, Fig. 36, indicates a markedly rougher surface for the extracted fibers. Electron diffraction performed on material protruding from the surface of the extracted fibers showed the presence of two separate phases. The more predominant of the two, observed on approximately 95% of the examined fiber surface, was lithium spinel ($Li_2O \cdot 5Al_2O_3$, ASTM Card No. 3-0911), Fig. 37. The remaining 5% of the fiber surface was randomly covered with thin, single crystal platelets rendering a diffraction pattern as given in Fig. 38. Attempts to identify these single crystals as a reaction phase of the fiber and matrix were not successful. It is therefore suspected that the platelets are a reaction product precipitated out of the extracting solution.

E. Composite Tensile Properties

Selected specimens, representing various degrees of composite infiltration and matrix alloy composition, were tensile tested to determine composite tensile strength, and in selected cases, elastic modulus and strain to failure. Only specimens which were fabricated using fiber FP-IV were tested. Tensile test data are presented in Table IV for all of the specimens tested. In all but two cases the fiber content was maintained in the 50-60%, by volume, range.

The fracture surfaces of specimens containing 50% and 34% fiber are shown in Figs. 39 and 40 respectively. The matrix alloy for these specimens contained 2% lithium and infiltration was complete in both cases except for the presence of some voids on one edge of the lower fiber content specimen. The fracture surfaces consisted of large regions in which there was almost no evidence of individual fiber pull out, and local matrix failure appeared to be by shear between the fibers, Fig. 41. A degree of fracture surface roughness was introduced by steps, some of which extended over large regions, Fig. 42. The walls of these steps contain evidence of fiber-matrix debonding, i.e. uncoated fibers or matrix

with the characteristic impressions of previously present fibers. Apparently, as cracks propagated across the specimen cross section, they were diverted at these boundaries of low fiber-matrix strength. Except for these rather small diversions of the fracture plane, there is little evidence for any ability of these composites to resist crack growth.

The stress strain curves obtained from specimens containing 50% and 34% FP-IV fiber are presented in Figs. 43 and 44 respectively. In both cases the curves were bilinear with the initial portion corresponding to elastic deformation of both matrix and fiber. Matrix yield occurred at a strain of 0.03-0.04% and thereafter the composite elastic modulus was decreased due to occurrence of plastic deformation of the matrix. Both the primary and secondary elastic moduli agree with a simple rule of mixtures calculation to within 10%. The specimens were each also cycled once during loading prior to failure to illustrate the change in yield point due to work hardening of the matrix.

The values of composite strength and failure strain for the two sets of specimens obtained from alloy number 19 can be used to estimate the fiber bundle strength in these composites. The average failure strain for composites containing 50% and 32-34% fiber is 0.26%. This value should be the same for both percentages of fiber, because final failure should be fiber controlled in both cases. Using this value of strain, and the fiber elastic modulus of 345 GPa, it is calculated that the effective fiber bundle strength is approximately 900 MPa. Based on this value, and assuming elastic deformation of the aluminum matrix (which is not true but close enough for this approximation), it can be predicted that the fracture strengths of the 50% and 32-34% fiber composites should be 540 MPa and 415 MPa respectively. The former value agrees very well with observation while the latter is high by about 30%. The total number of composite specimens tested, however, is too few to make a more definitive comparison.

An independent estimate of fiber effective bundle strength was made using the data for FP-IV fibers presented in Fig. 2. Based on the statistical distribution of strengths, bundle strengths of 880 MPa and 1120 MPa were calculated for strength populations including kinked fiber failures, and excluding kinked fiber failures, respectively. These values are both in reasonable agreement with the value of 900 MPa obtained above from the composite data.

Further fractographic investigation indicated that, for specimens containing higher percentages of lithium, the degree of fiber pull out and surface roughness decreased even further with no apparent detrimental effect on composite axial strength, Fig. 45. Similarly, alloying with magnesium and maintaining a high enough level of lithium caused no discernible change in fracture appearance, Figs. 46 and 47.

The importance of lithium content is also observable in specimens with lower percentages. Specimen 14-2, Fig. 48, is shown as an example. With 1.1% lithium the fiber-matrix bond strength was apparently adversely affected causing much larger steps on the fracture surface. Small local areas of incomplete infiltration are also evident through the presence of isolated fibers protruding well above the fracture plane. Although the degree of bonding was significantly altered, the axial strength was very similar to that of specimens containing higher percentages of lithium.

Finally, those specimens which did not contain any lithium, although infiltrated at least on a macro scale, exhibited a very large change in fracture mode. The apparent lack of bonding between fiber and matrix caused very large longitudinal splits to occur at relatively low applied stress levels. The specimens then just continued to splinter and pull apart, Fig. 49, rather than fail in a normal tensile mode.

In general, it was found that low strength specimens could be associated with incomplete infiltration of the composite and large areas of poor fiber-matrix bonding. This type of behavior occurred not only for matrices which did not contain lithium, but also for several cases where the overall lithium content of the matrix was high enough, but other conditions, such as melt temperature, were not optimum.

IV. DISCUSSION AND CONCLUSIONS

It has been demonstrated that high strength metal matrix composites can be fabricated easily using several simple liquid metal infiltration processes. Although more than one matrix composition infiltrated the preform arrays of fibers, it is clear that low strength composites will result unless a significant amount of fiber-matrix wetting takes place. Without this wetting, by reaction between the composite constituents, the composite contains small pores in the final structure and a low strength fiber-matrix bond. Both of these defects will lead to low off-axis strength and, as shown in this report, they also prevent the achievement of high axial strength.

The use of lithium in the aluminum melt satisfied all requirements to achieve a well infiltrated composite with FP alumina fibers. It was also demonstrated, however, that the percentage of lithium could be reduced through the use of magnesium as a second alloying addition. This combination of alloying elements may also prove useful in the future in achieving a high strength heat treatable matrix.

By the use of secondary ion mass spectrometry and transmission electron microscopy of the surface of fibers extracted from infiltrated composites, it was demonstrated that only lithium reacted significantly with the alumina fibers. The magnesium and bismuth did remove the thin silica layer present on FP-IV fibers, however, these elements did not react with the alumina fiber itself. The lithium-alumina reaction was determined to extend into the surface of the fiber leaving a surface reaction product of $Li_2O \cdot 5Al_2O_3$. This reaction did not, however, degrade the fiber strength. This was illustrated by a comparison between as-received fiber bundle strength and the in-situ fiber strength, determined on the basis of measured composite strength and strain to failure. An effective fiber strength of approximately 900 MPa was determined to be typical of fiber FP-IV.

The relative ease with which composites could be cast was found to be very encouraging. It should now be possible to take advantage of metal casting technology to achieve metal matrix composite articles previously not readily fabricable by standard hot pressing procedures. The use of a selective reinforcement technique, using aluminum wires as a filler, has also demonstrated a feasibility for controlled placement of the reinforcing fiber which may prove advantageous in cost controlled industrial applications. Circumferentially wrapped tubes and selectively stiffened gear box housings are just two examples of articles previously not readily fabricable using boron reinforced aluminum which can now be actively considered.

A composite containing 50% FP fiber with an axial tensile strength of 550 MPa, axial elastic modulus of 200 GPa, and a density of 3.3 gm/cc that is castable and low cost should be very attractive for large scale composite use. Although clearly not competitive with boron aluminum, on a specific property basis, FP-aluminum's fabricability and low cost potential should provide it with an industrial market far in excess of that reserved for this higher performance system.

REFERENCES

1. A. A. Baker, D. Cratchley: App. Mat. Res., p. 251, Oct. 1964.
2. D. Cratchley, A. A. Baker: Metallurgia, Vol. 69, p 153, 1964.
3. A. A. Baker, D. Cratchley: App. Mat. Res., p 92, April 1966.
4. A. A. Baker: Ibid., p 210, Oct. 1966.
5. A. A. Baker: J. of Mat. Sci., Vol. 3, p 412, 1968.
6. W. Fiedler, et al: Cont. NOrd-13484, AFOSR, 1958.
7. P. A. Lockwood: Owens Corning Fiberglass Res. Center Report, 1959.
8. M. F. Amateau: "Progress in the Development of Graphite-Aluminum Composites by Liquid Infiltration Technology", Aerospace Co. Report ATR-76-8162-3, 1976.
9. A. K. Dhingra, et al: DuPont Report, 1974.
10. T. H. Sanders: Naval Air Development Center Contract N62269-74-C-0438, Final Report, June 9, 1976.
11. B. Noble and G. E. Thompson: Metal Science Jl., Vol. 5, p 114, 1971.
12. W. R. D. Jones, P. P. Das: Jl. Inst. of Metals, Vol. 88, p 435, 1959.
13. H. K. Hardy: Jl. Inst. of Metals, Vol. 84, p 429, 1955.
14. French Patent No. 1.161.306, Nov. 23, 1956.
15. "Aluminum", edited by K. R. Van Horn, ASM, 1967.
16. W. H. Sutton, et al: Final Report Contract NOw 64-0540c, 1965.
17. R. E. Tressler in "Interfaces in Metal Matrix Composites", ed. by A. G. Metcalfe, Academic Press, 1974.
18. A. E. Standage and M. S. Gani: Jl. Am. Cer. Soc., Vol. 50, p 101, 1967.
19. B. C. Pai, et al: Mat. Sci. and Engineering, Vol. 24, p 31, 1976.
20. W. H. Streuer and S. Kaye: Final Report Contract NAS8-27806, Jan. 1973.

Table I

Manufacturer's Fiber Data at 70°F

	Units	Dupont FP Type I	Dupont FP Type IV	Sumitomo	3M AB-312	Tyco* (single crystal)	Boron*
Diameter	Microns	15-25 (round)	15-25 (round)	11	10-12 (round)	250 (round)	140 (round)
Density	g/cm^3	3.95	3.95	3.1	2.7	3.97	
	$lb/in.^3$	0.142	0.142	0.112	0.097	0.143	0.09
Form Available		yarn	yarn	yarn	yarn & fabric	single filament	single filament
Length Available	m	continuous	continuous	.01	continuous	continuous	continuous
Commercial Available Price	$/lb	75 (current)	75	10-20 (anticipated)	25 (current)	15,000 ($2 per ft)	100-200
Composition		Al_2O_3	Al_2O_3 + SiO_2	Al_2O_3 + SiO_2	alumina boria silica	Al_2O_3	B
Maximum Long Term Use Temperature in Air	°C	1000°C	-	1350	1300	1300	-
Tensile Strength	10^6 N/m^2	1380	1720	2450	1720	2420	2760
	10^3 psi	200	250	355	250	350	400
Specific Tensile Strength	10^6 in.	1.41	1.76	3.17	2.58	2.45	4.45
Elastic Modulus	10^9 N/m^2	345	345	290	159	462	380
	10^6 psi	50	50	42	23	67	55
Specific Elastic Modulus	10^8 in.	3.50	3.50	3.75	2.37	4.68	6.1
Surface Area	m^2/gm	-	-	<10	1	-	-

*These fibers were not used in the program but are just presented for comparison

Table II

Alloy Compositions Investigated
(Weight Percent Elements)

Alloy	Al	Li	Mg	Bi	Zr	Melt Designation
Pure Al	99.9	-	-	-	-	8
Al-Li	Bal	4	-	-	-	1
	"	4	-	-	-	2
	"	2	-	-	-	3
	"	2.7	-	-	-	4
	"	2.0	-	-	-	5
	"	2.3	-	-	-	6
	"	2	-	-	-	7
	"	2	-	-	-	11
	"	2.5	-	-	-	19
Al-Bi	Bal.	-	-	2	-	9
Al-Mg	Bal.	-	10	-	-	10
	"	-	12	-	-	12
Al-Mg-Li	Bal.	1.5	12	-	-	13
	"	1.5	7	-	-	14
	"	0.5	7	-	-	15
	"	0.5	12	-	-	16
	"	2.5	4	-	0.12	17
	"	1.5	4			18

Table III

Analyzed Alloy Compositions Investigated
(Weight Percent Elements)

Alloy	Al	Li	Mg	Bi	Fe	Zr	Ni	Cr	Melt Designation
Pure Al	99.9	-	-	-	-	-	-	-	8
Al-Li	Bal.*	Nom. 4%	-	-	-	-	-	-	1
	"	3.3	0.07	<0.03	0.65	-	0.06	0.06	2
	"	1.6	0.08	<0.03	1.0	-	0.2	0.2	3
	" *	Nom. 2.7	-	-	-	-	-	-	4
	" *	Nom. 2.0	-	-	-	-	-	-	5
	"	1.5	0.05	<0.03	1.1	-	0.24	0.43	6
	"	1.2	0.03	<0.03	1.8	-	0.27	0.03	7
	" *	Nom. 2.0	-	-	-	-	-	-	11
	"	2.0	0.05	<0.03	0.9	-	0.13	0.15	19
Al-Bi	Bal.	<0.003	0.01	1.4	2.0	-	0.25	0.50	9
Al-Mg	Bal.	-	Nom. 10	-	-	-	-	-	10
	Bal.	-	Nom. 12	-	-	-	-	-	12
Al-Mg-Li	Bal.	1.0	11.0	<0.03	0.5	-	0.1	0.2	13
	"	1.1	5.8	<0.03	0.3	-	0.06	0.1	14
	"	0.5	5.3	<0.03	1.4	-	0.15	0.4	15
	"	0.4	10.4	<0.03	0.5	-	0.08	0.16	16
	"	1.2	3.7	<0.03	0.7	0.08	0.1	0.1	17
	"	1.7	4.0	<0.03	0.5	-	0.09	0.14	18

*These alloys were not chemically analyzed so the data are nominal compositions

Table IV

Composite Tensile Test Data
(FP-IV Fiber in All Cases)

Matrix Alloy	Volume Percent Fiber %	Specimen Number	Axial Tensile Strength MPa	Axial Tensile Strength 10^3 psi	Axial Elastic Modulus GPa	Axial Elastic Modulus 10^6 psi	Axial Failure Strain %
Al-3.3% Li	55	2-10	355	51.5			
	55	2-12	486	70.5			
	55	2-13	449	65.1			
	55	2-14	407	59.1			
Al-1.6% Li	60	3-1	495	71.9			
	60	3-2	440	64.0	206	29.8	0.22
	60	3-3	508	73.8			
	60	3-4	402	58.3			
	60	3-5	360	52.2			
Al-2% Li	60	5-6	439	63.7			
Al-1.5% Li	50	6-1	257	37.3			
	50	6-4	523	75.9			
	50	6-13	546	79.3			
	50	6-15	519	75.3			
	50	6-17	477	69.2			
Al-1.2% Li	57	7-2	453	65.8			
Al-2% Li	50	19-26	584	84.6	204	29.6	0.30
	50	19-28	529	76.7	198	28.8	0.27
	32	19-8	283	41.1	149	21.6	0.20
	34	19-10	349	50.6	149	21.7	0.26
Al-1.4% Bi	58	9-20	308	44.6			
	58	9-21	289	42.0			
Al-1%Li-10%Mg	50	13-6	379	55.0			
Al-1.1%Li-5.8%Mg	55	14-2	515	74.7			
	55	14-3	346	50.3			
Al-0.5%Li-5.3%Mg	55	15-3	>451	>65.4			
Al-0.4%Li-10.4%Mg	53	16-1	398	59.5			
	53	16-3	403	57.7			
Al-1.2%Li-3.7%Mg	55	17-2	565	81.9			
	55	17-3	617	89.5			
	55	17-4	>579	>84.0			
	55	17-5	595	86.2			
	55	17-6	473	68.6			
Al-1.7%Li-4.0%Mg	55	18-1	571	82.8			

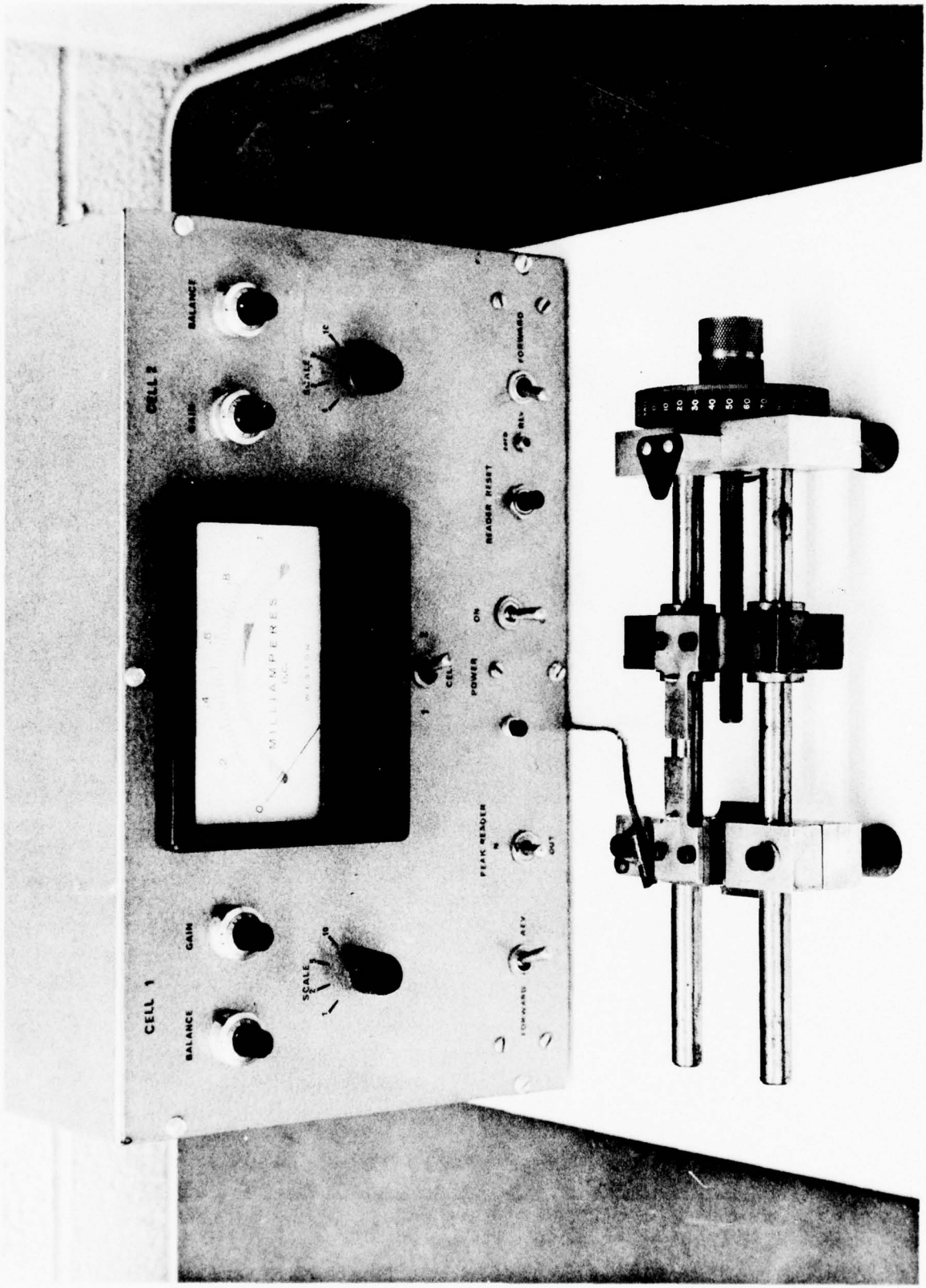

FIG. 1 FIBER TENSILE TESTER

76-03-155-4

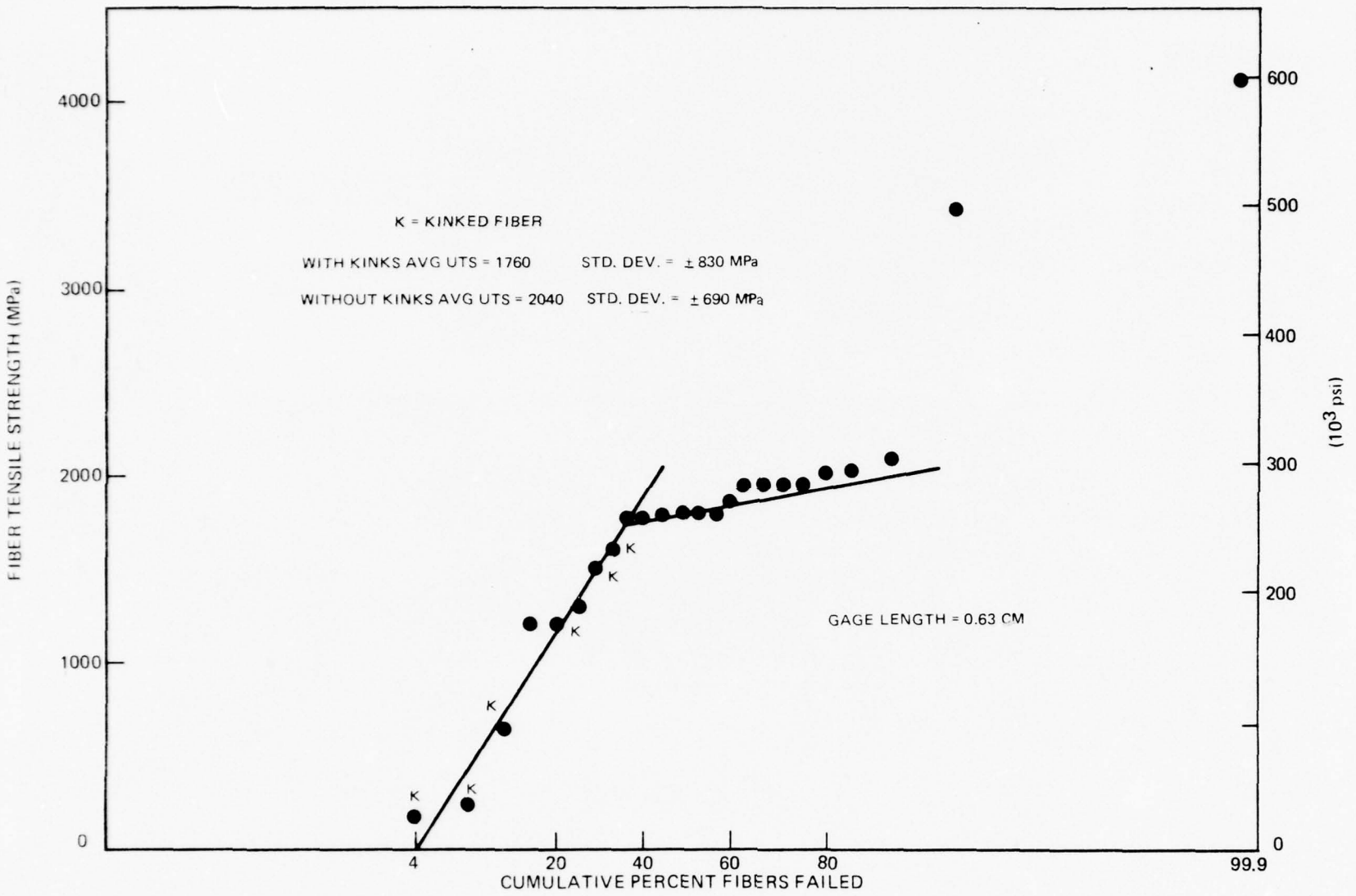

FIG. 2 FP FIBER (TYPE IV) STRENGTH DISTRIBUTION

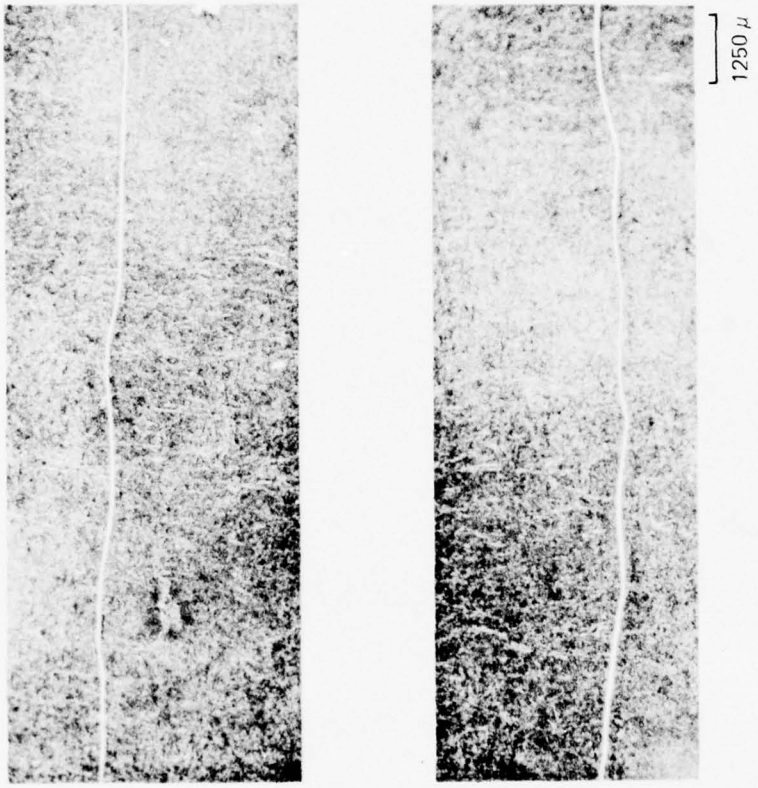

FIG. 3 KINKED FP FIBERS

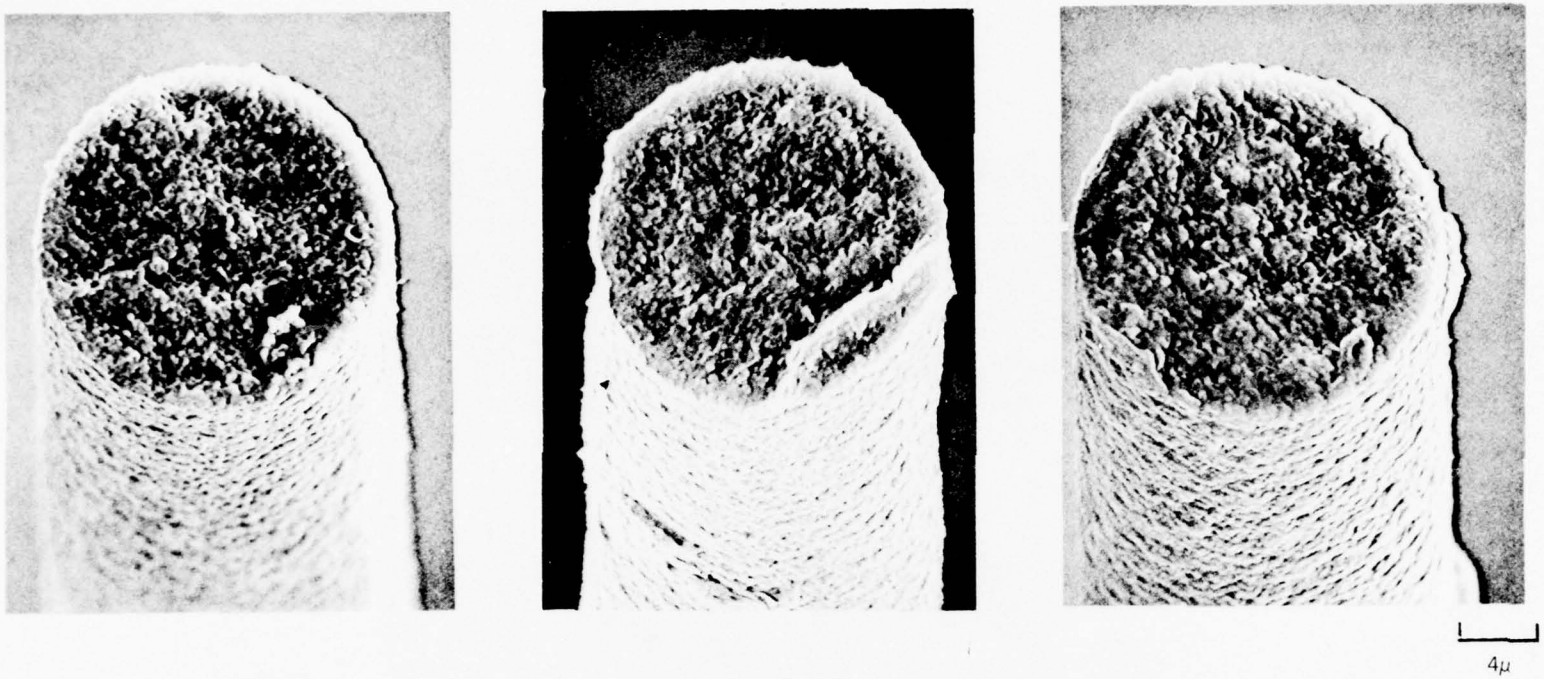

UTS = { 648 MPa / 94,000 PSI

UTS = { 2,100 MPa / 305,000 PSI

UTS = { 4,175 MPa / 600,000 PSI

FIG. 4 FP FIBER FRACTURE SURFACES

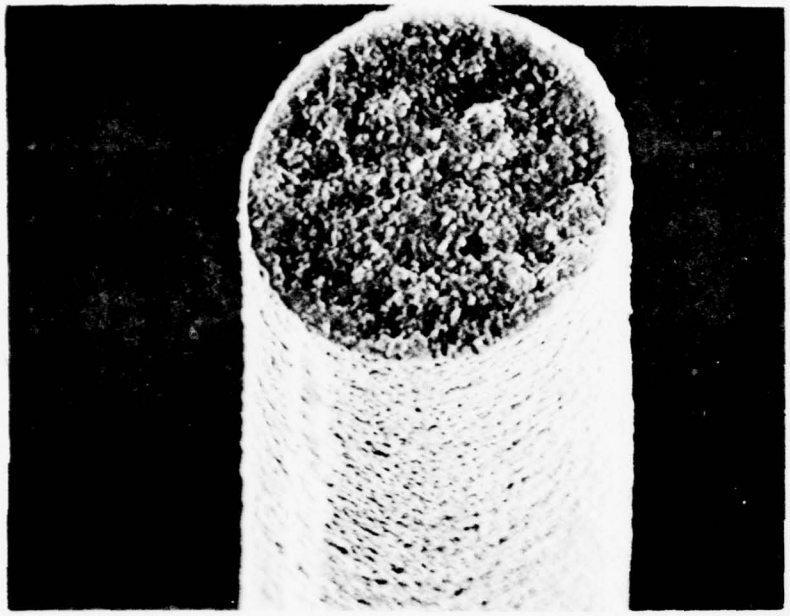

4μ

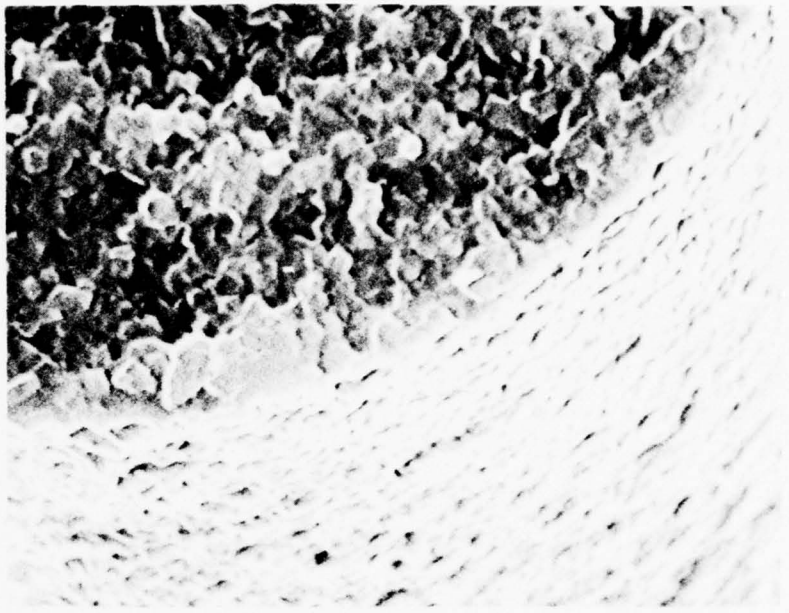

1μ

UTS = { 1,950 MPa
283,000 PSI

FIG. 5 FP FIBER FRACTURE SURFACE

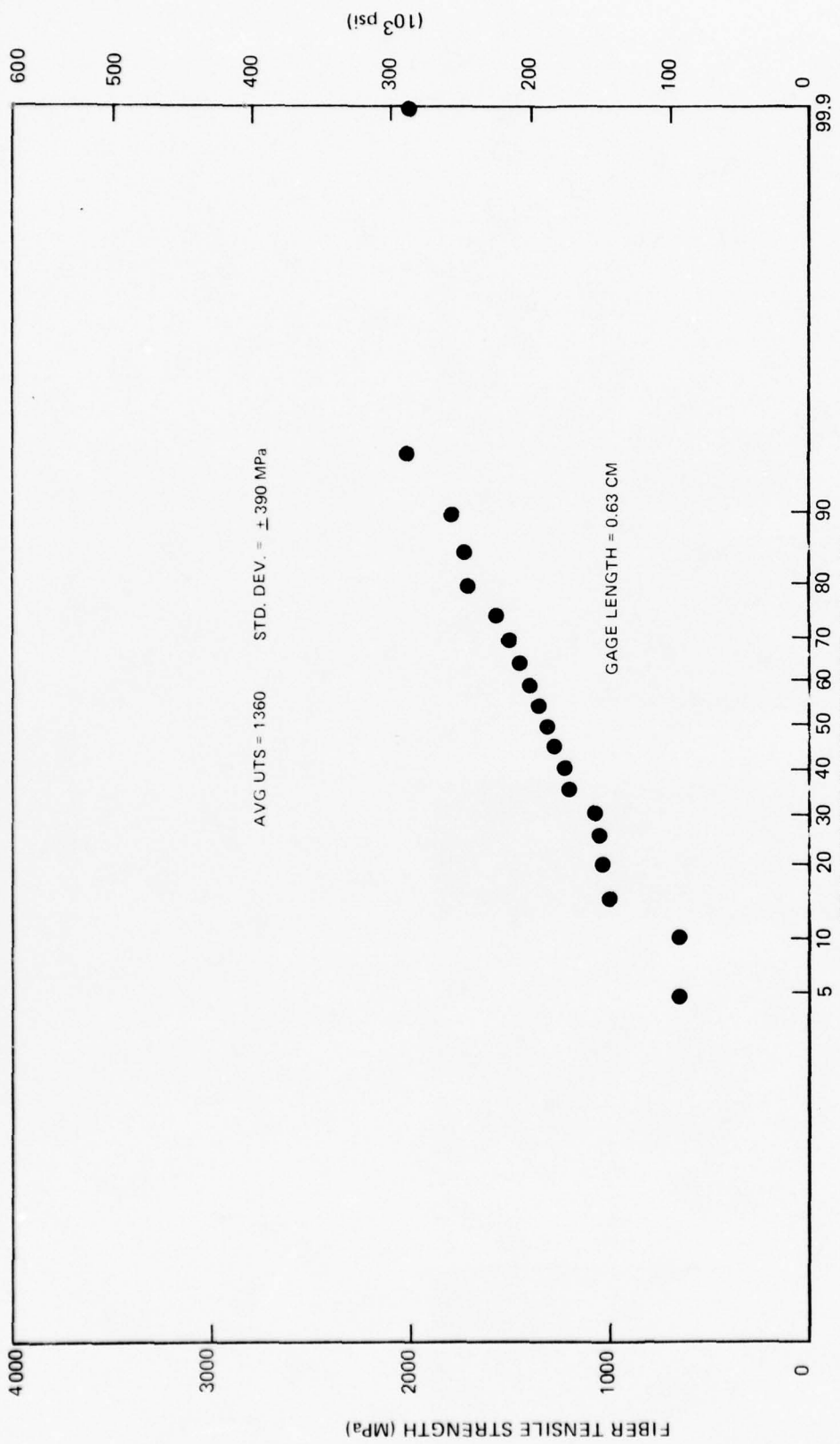

FIG. 6 AB 312 FIBER STRENGTH DISTRIBUTION

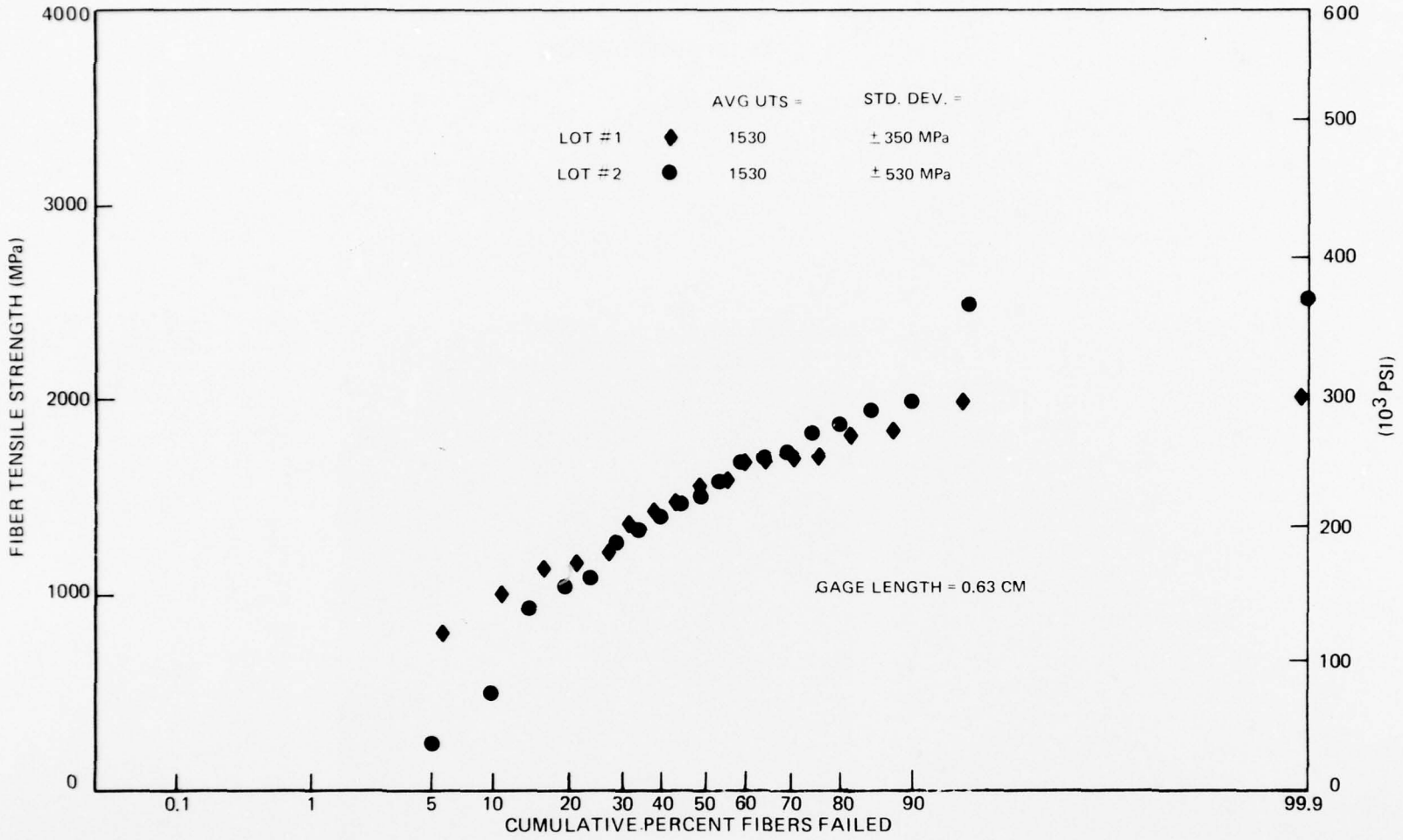

FIG. 7 SUMITOMO FIBER STRENGTH DISTRIBUTION

FIG. 8 FIBER SURFACES

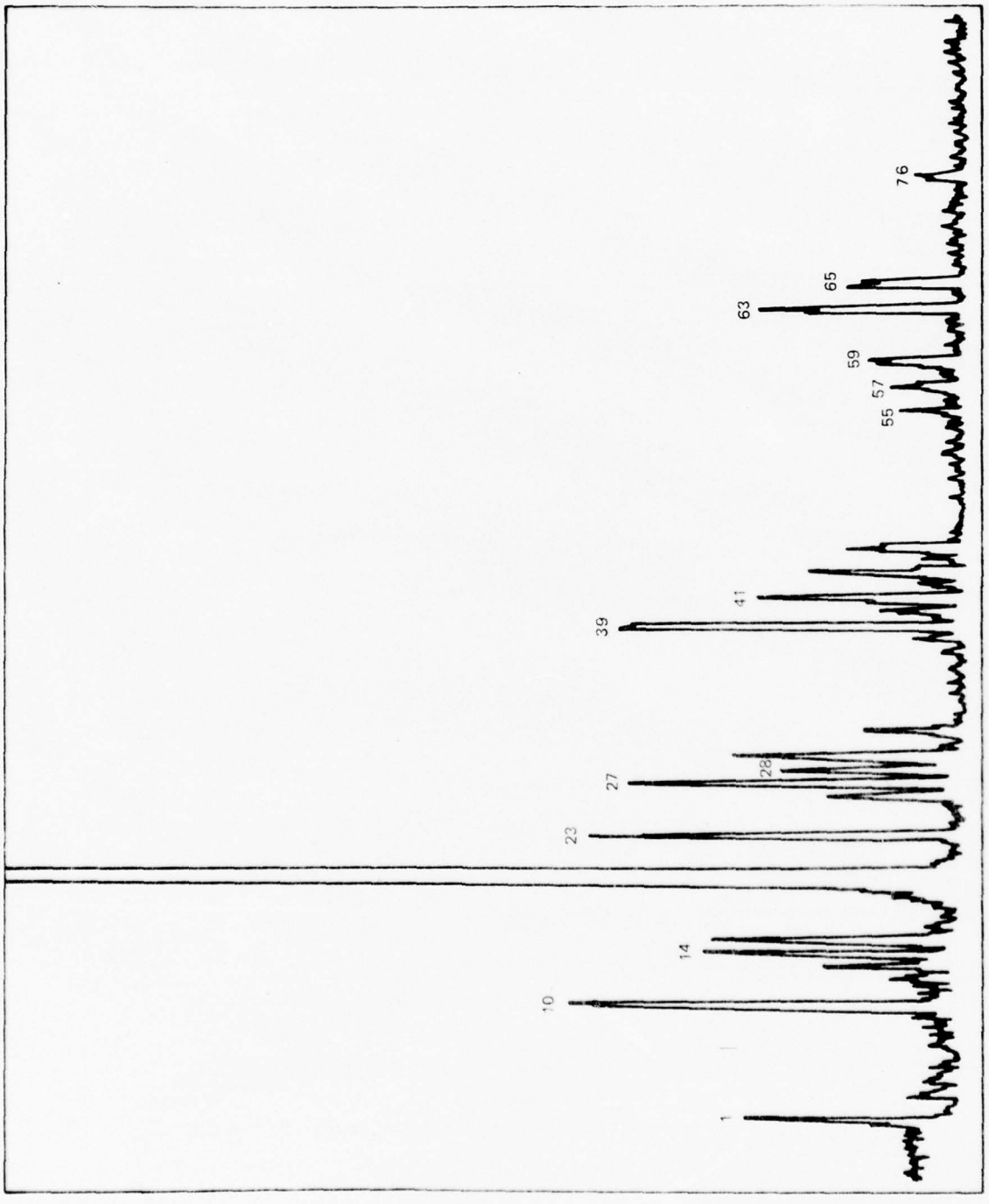

FIG.9 SIMS MASS SPECTRUM FOR AS RECEIVED FP-I FIBER

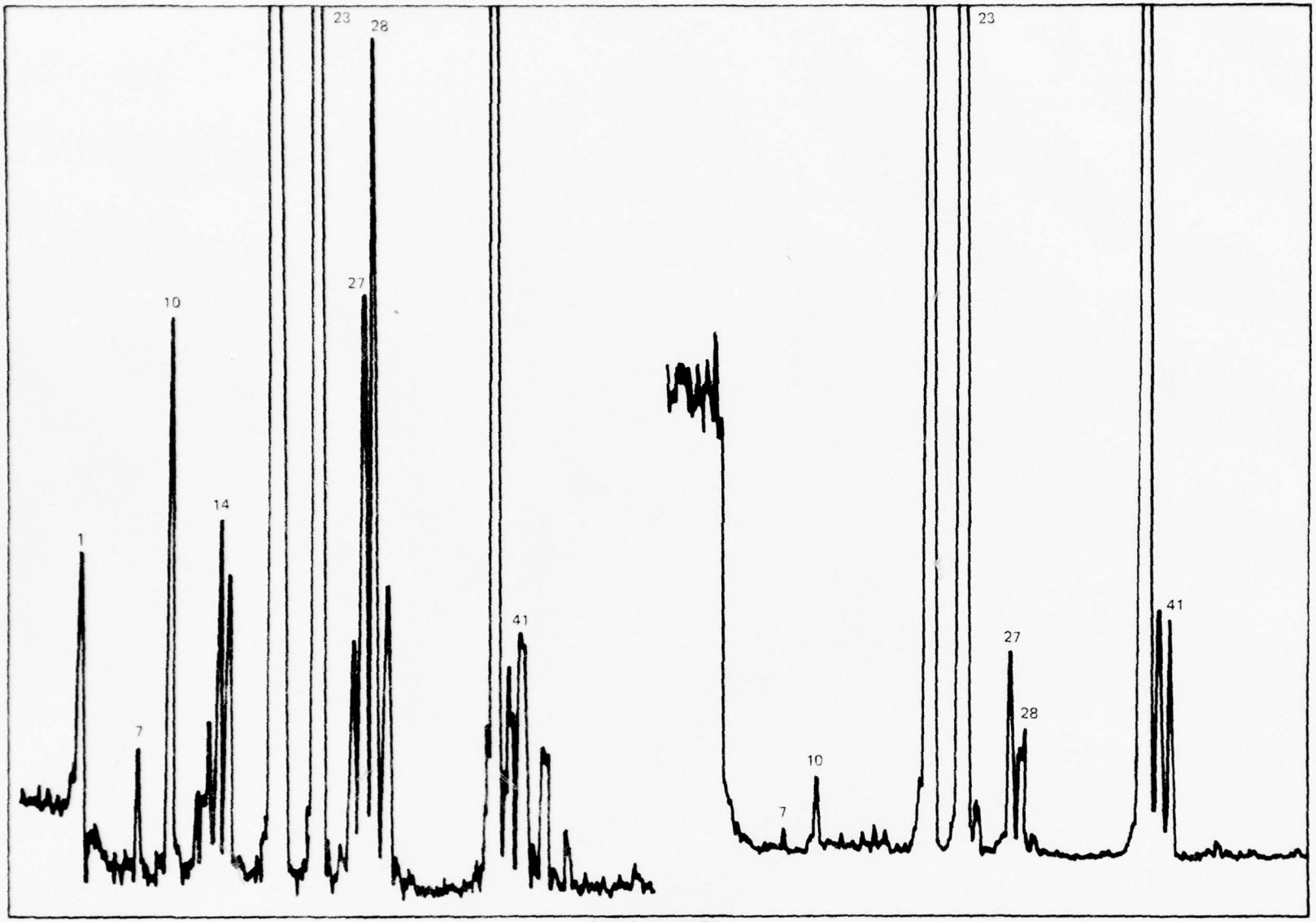

FIG.10 SIMS MASS SPECTRA FOR AS RECEIVED FP–IV FIBER

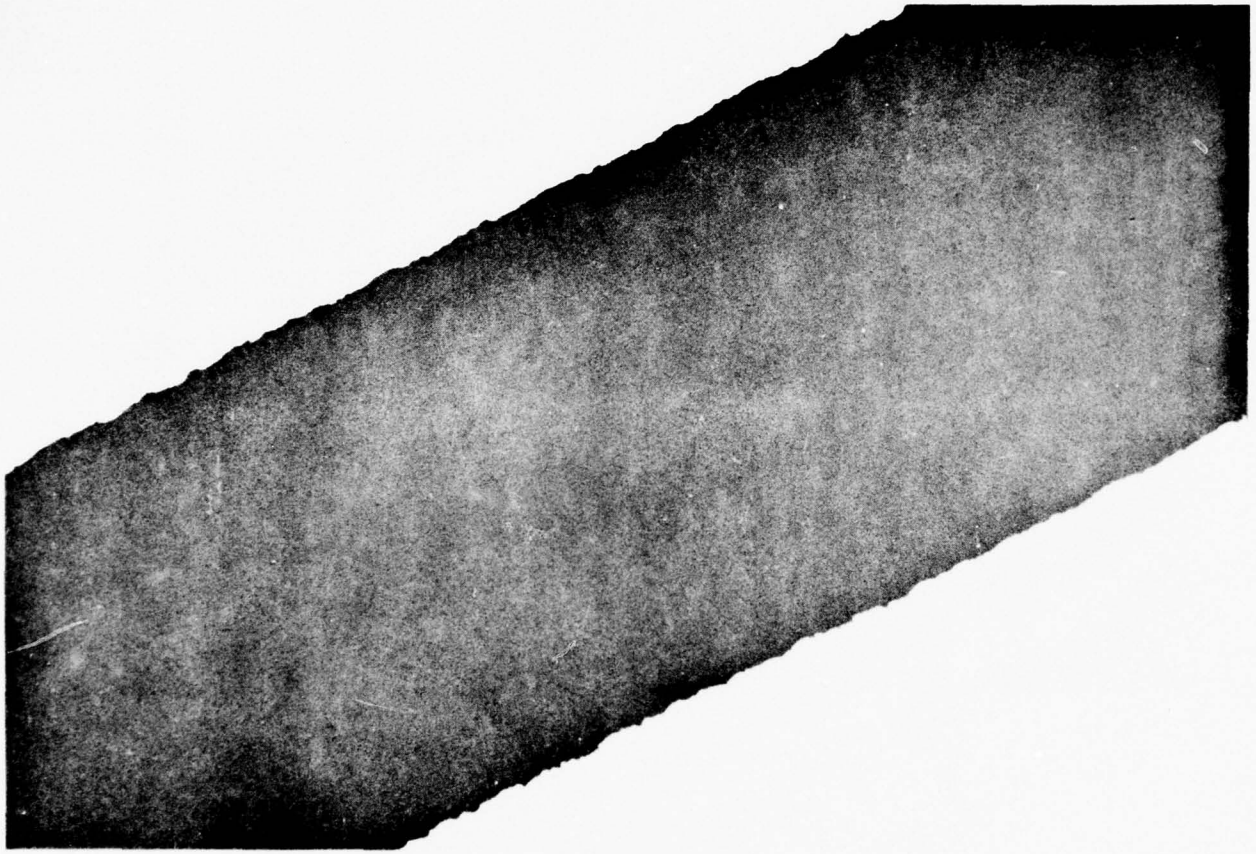

2μ

FIG. 11 PROFILE VIEW OF AS RECEIVED FP-IV FIBER AND ELECTRON DIFFRACTION PATTERN OBTAINED FROM FIBER SURFACE

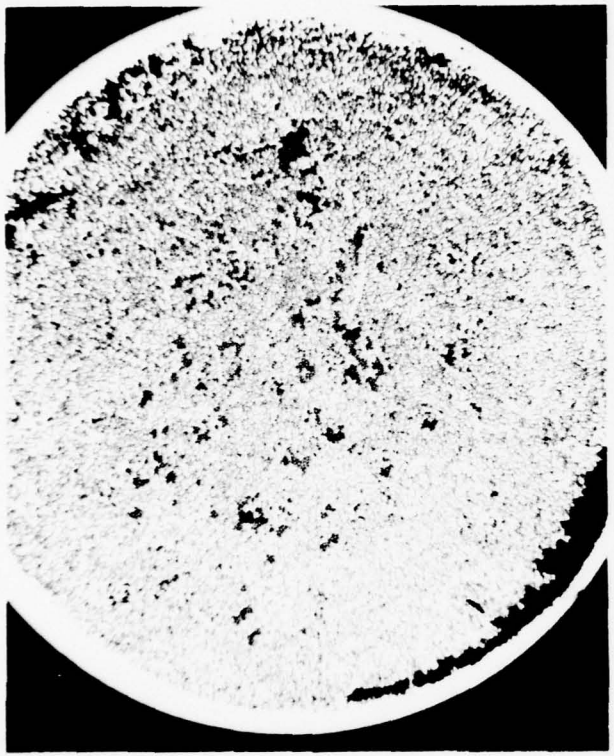

SPECIMEN 1-22
721°C

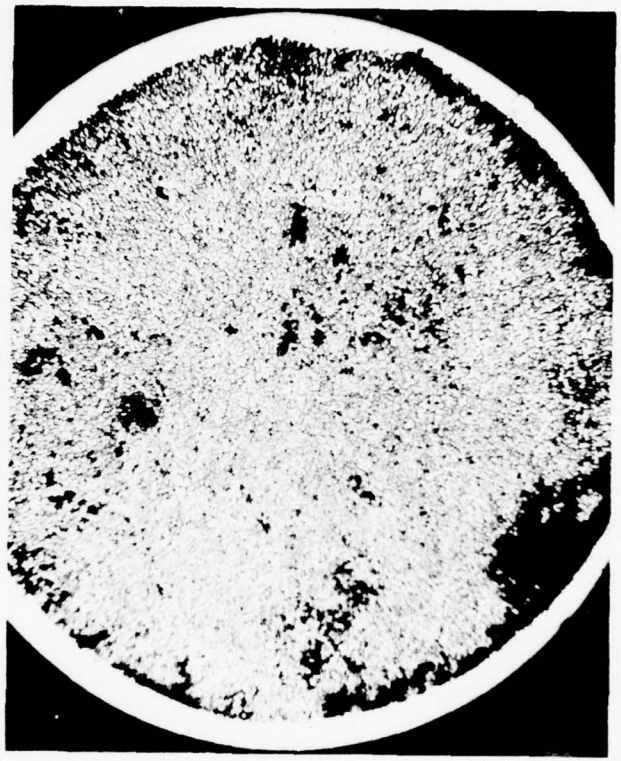

SPECIMEN 1-23
700°C

FIG. 12 EFFECT OF INFILTRATION TEMPERATURE FOR FPIV/Al-4% Al

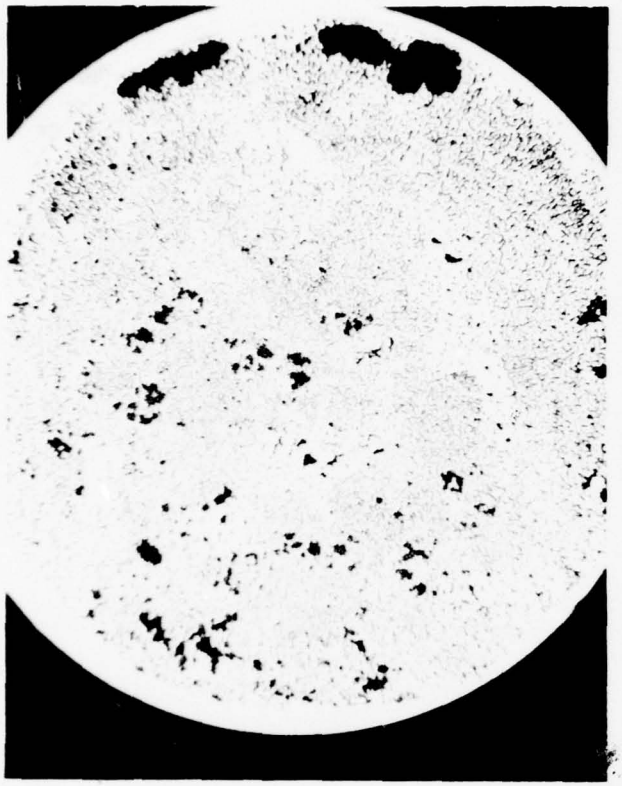

SPECIMEN 1–14
30% FP

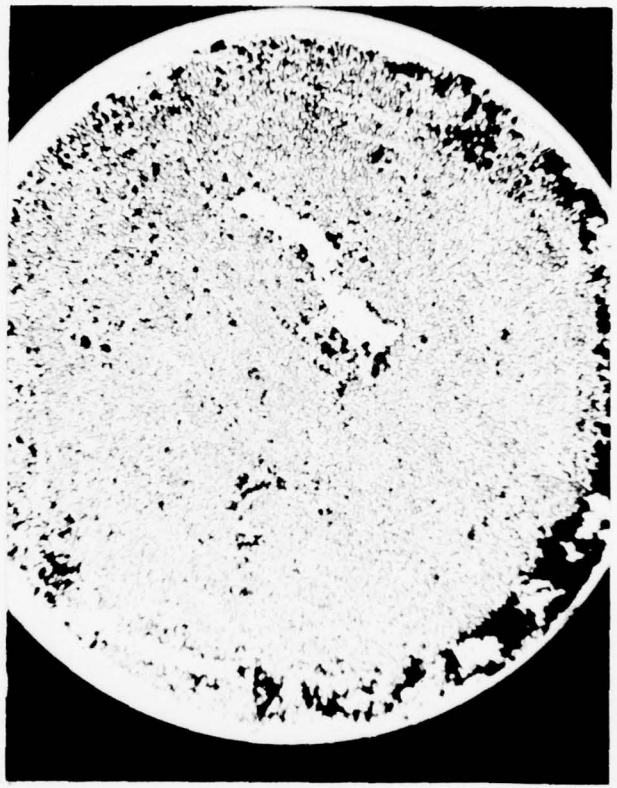

SPECIMEN 1–15
40% FP

FIG. 13 EFFECT OF VOLUME PERCENT FIBER FOR FPIV/Al–4% Li

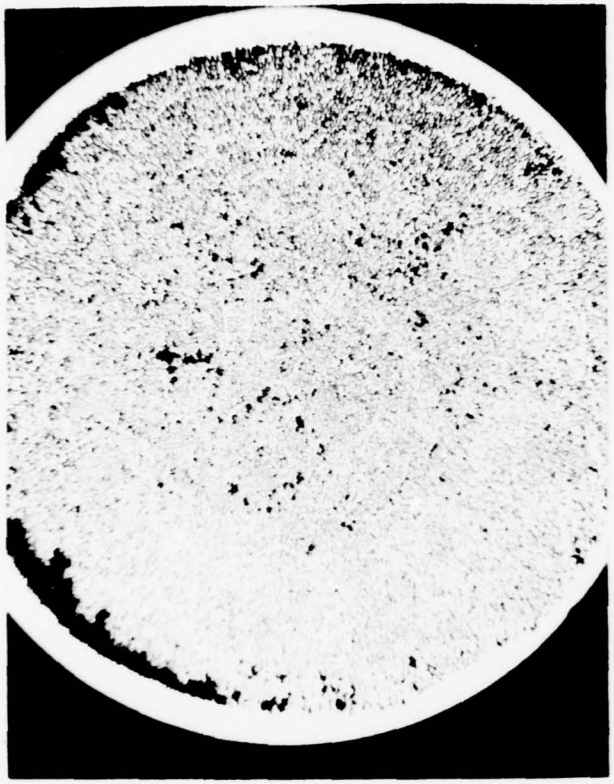

SPECIMEN 1-16
50% FP

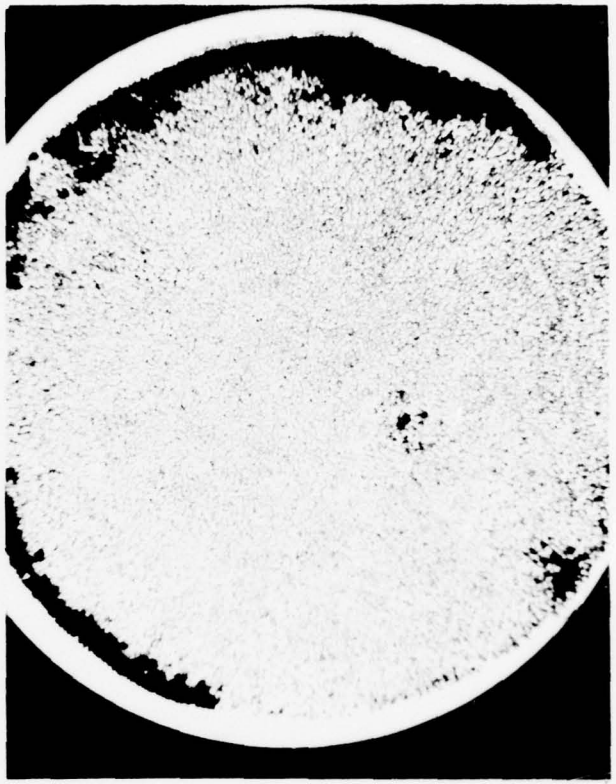

SPECIMEN 1-17
60% FP

FIG. 14 EFFECT OF VOLUME PERCENT FIBER FOR FPIV/Al-4% Li

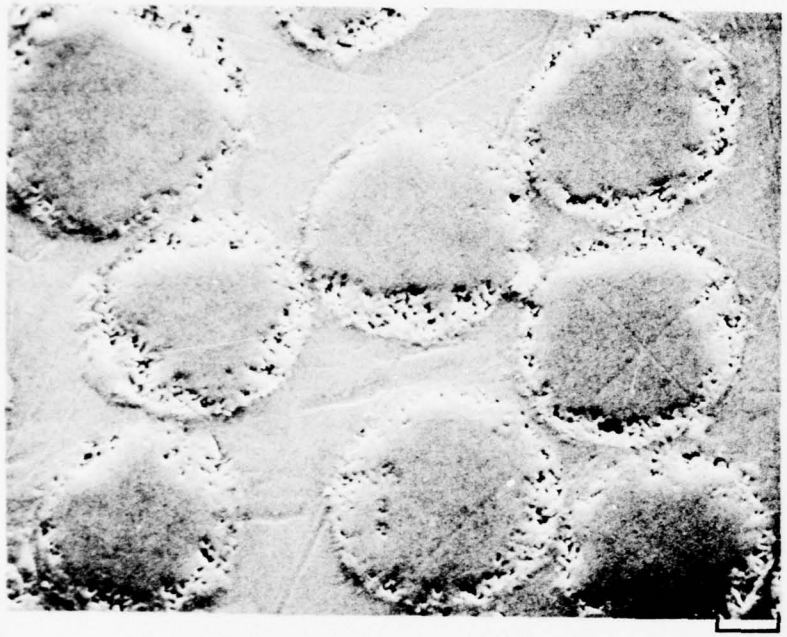

5μ

SPECIMEN – 10

(HELD FOR 15 SECONDS)

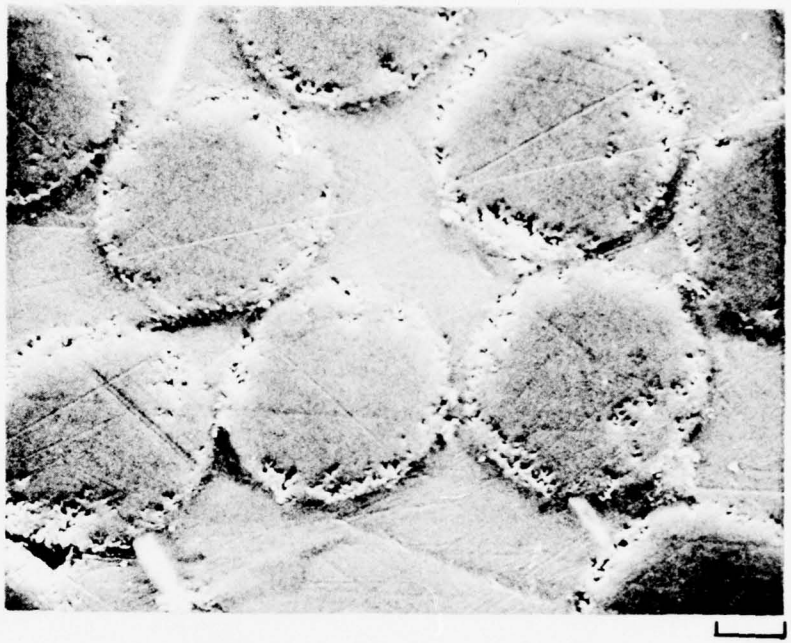

5μ

SPECIMEN 1–12

(HELD FOR 60 SECONDS)

FIG. 15 FP–IV/Al–4% Li

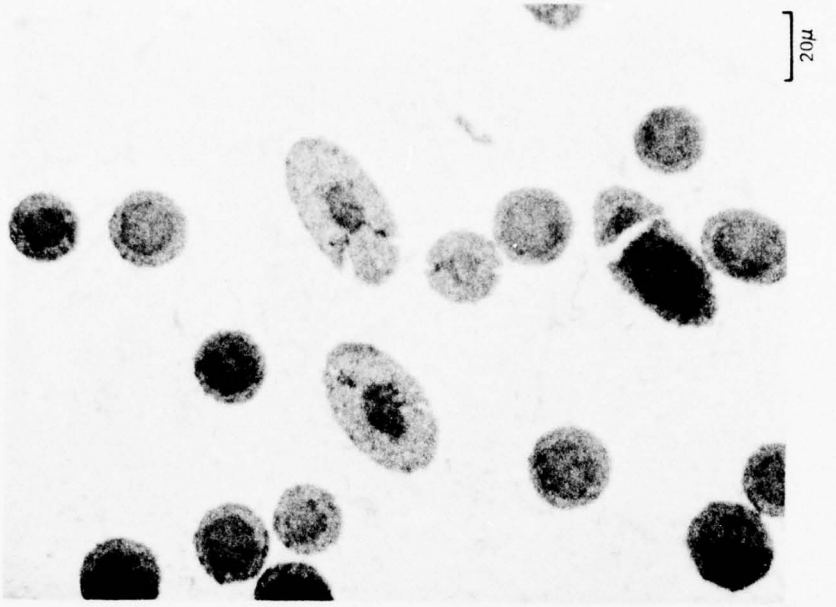

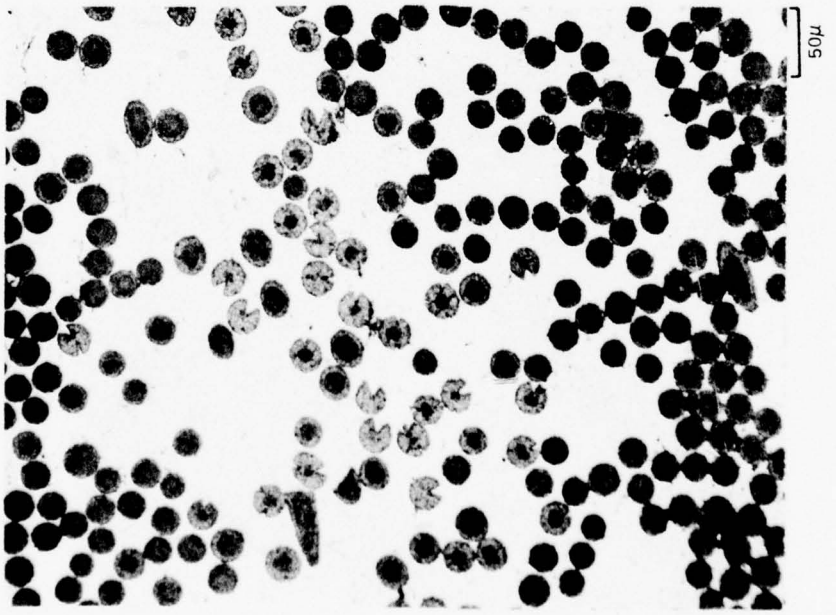

FIG. 16 OVER REACTED FP–IV FIBERS IN AN Al–4% Li MATRIX

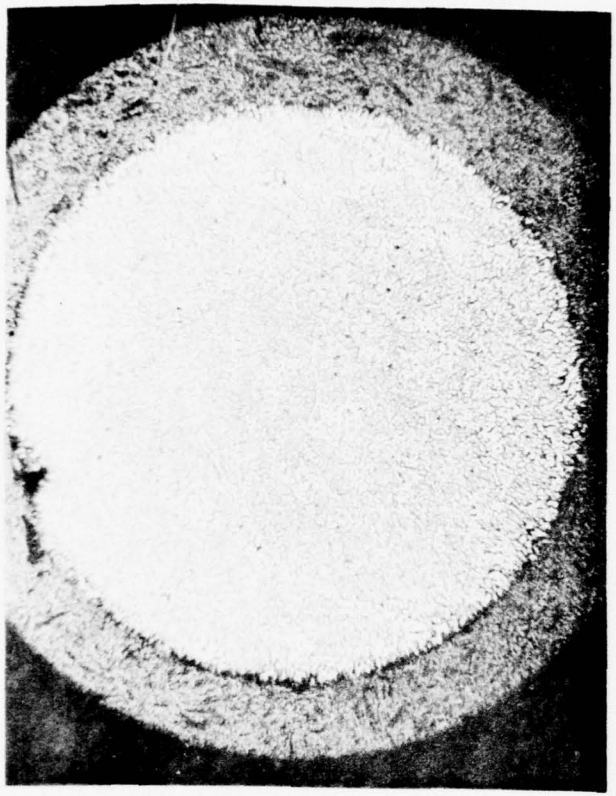

SPECIMEN 19–28
50% FIBER

500μ

SPECIMEN 19–28
30% FIBER

500μ

FIG. 17 FP–IV/Al–2.5% Li SPECIMENS FABRICATED BY PRE–EVACUATION

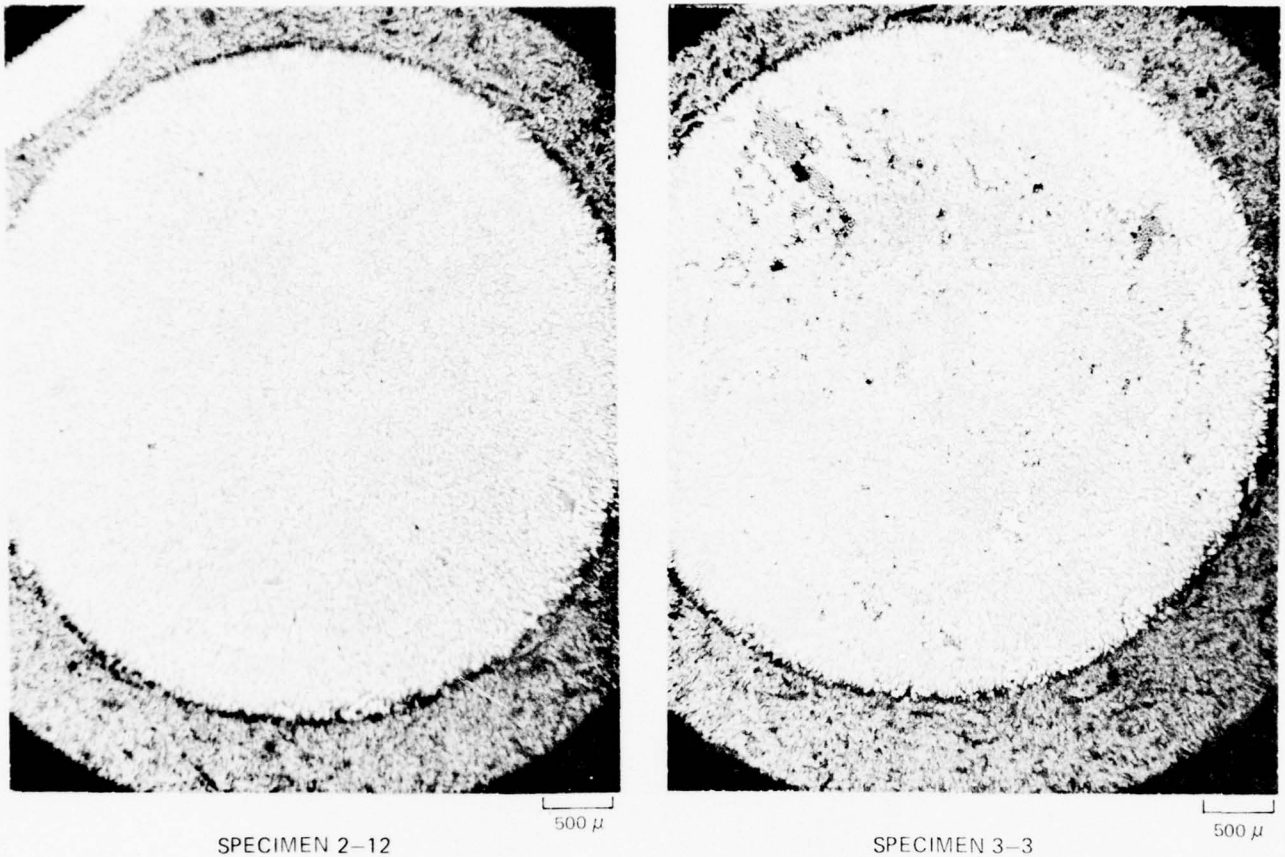

SPECIMEN 2–12
Al–3.3% Li

SPECIMEN 3–3
Al–1.6% Li

FIG. 18 FP–IV FIBER REINFORCED MATRICES INFILTRATED AT 720°C

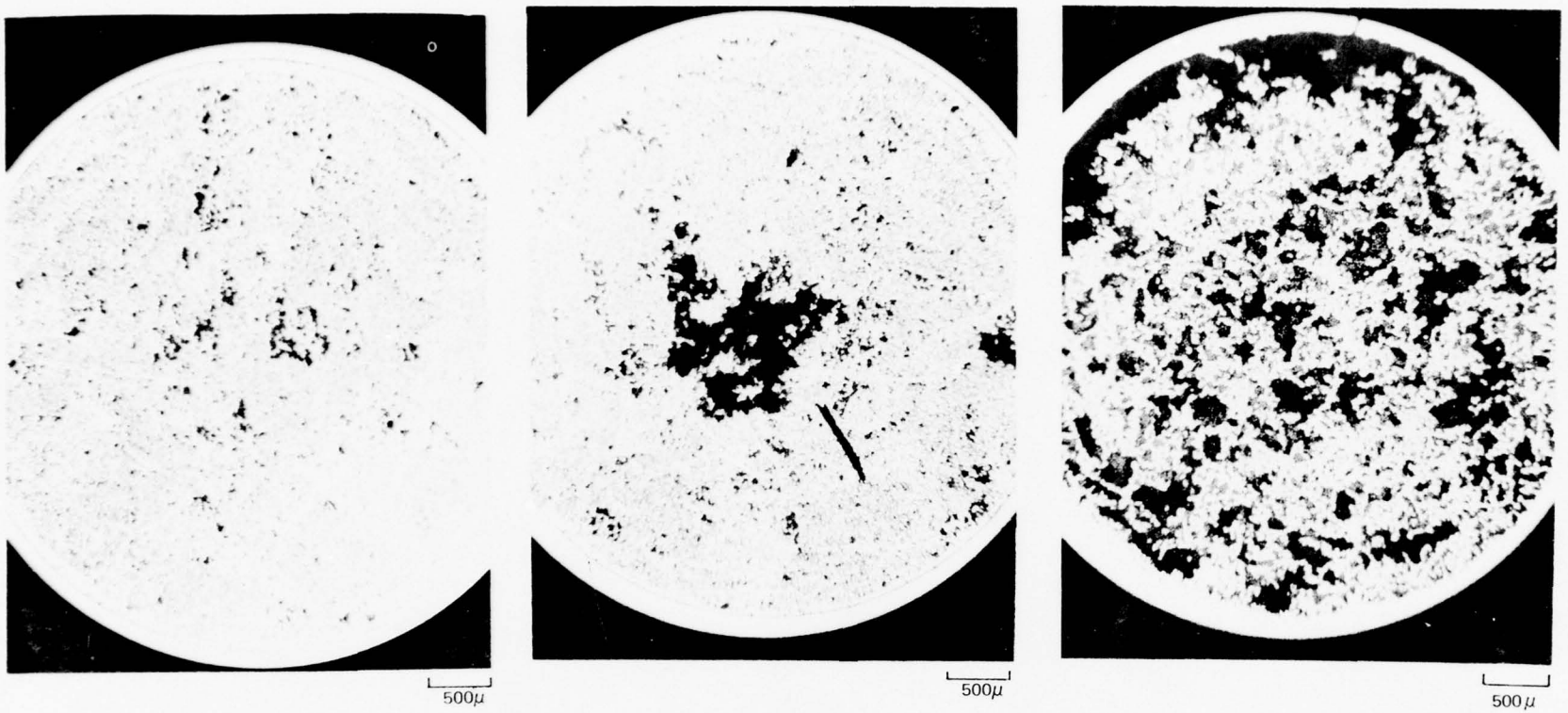

END NEAREST MELT

MID SPECIMEN

END FURTHEST FROM MELT

FIG. 19 FP–IV/Al–1.2% Li SPECIMEN 7–7 SECTIONED AT THREE LOCATIONS

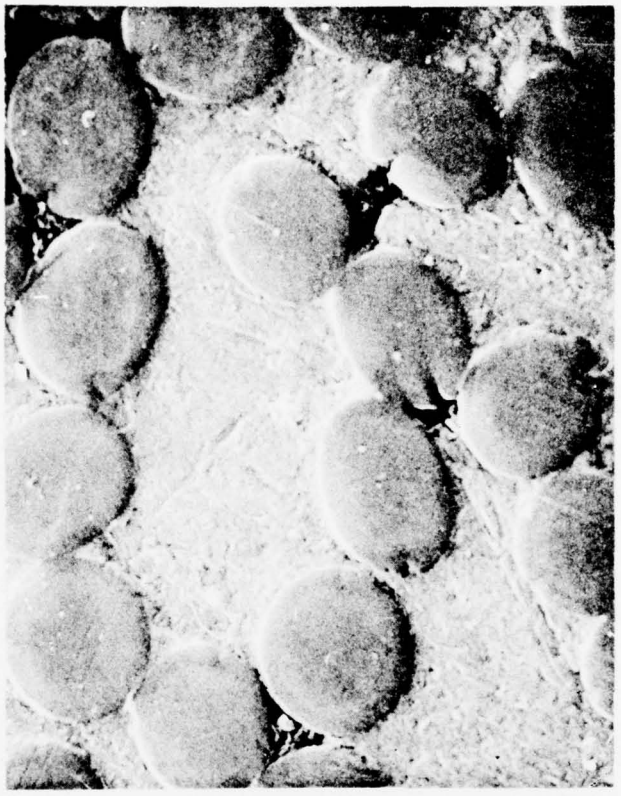

FIG. 20 AB-312/Al-4% Li

SPECIMEN 1 – 20

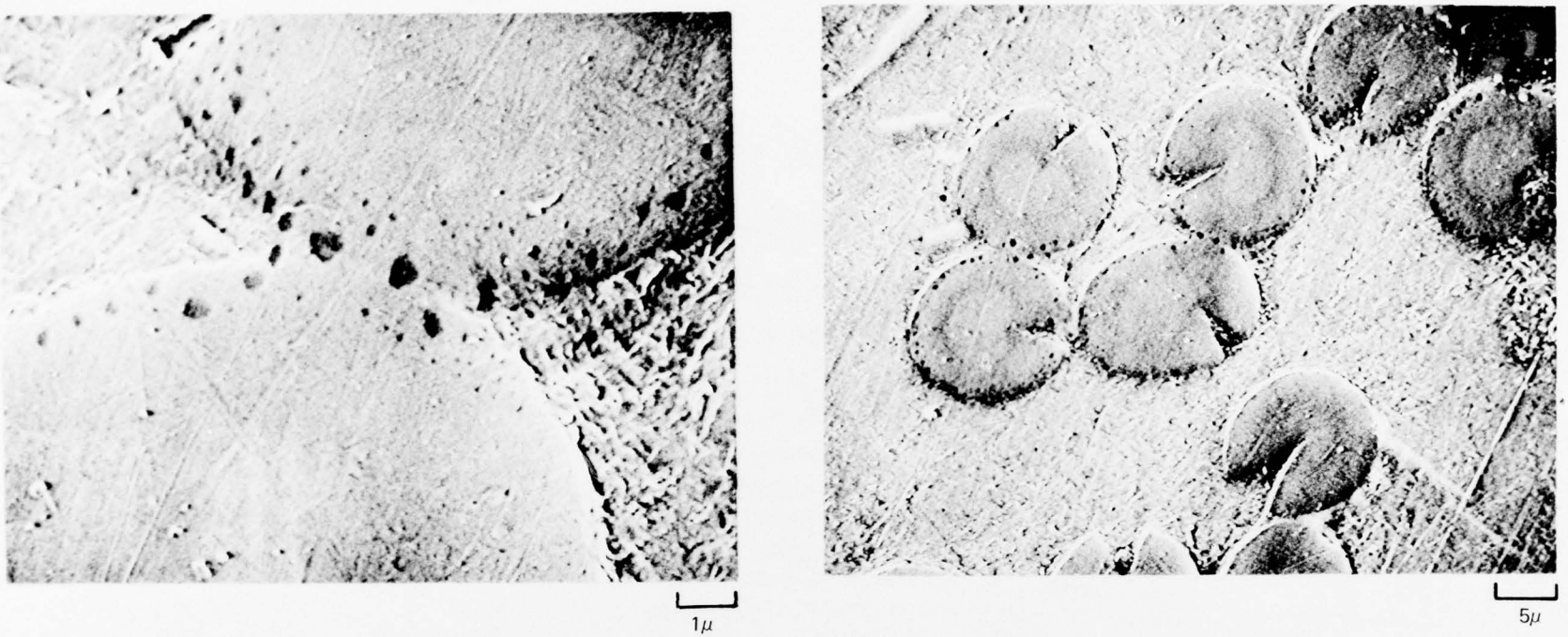

FIG. 21 AB–312/Al–4% Li

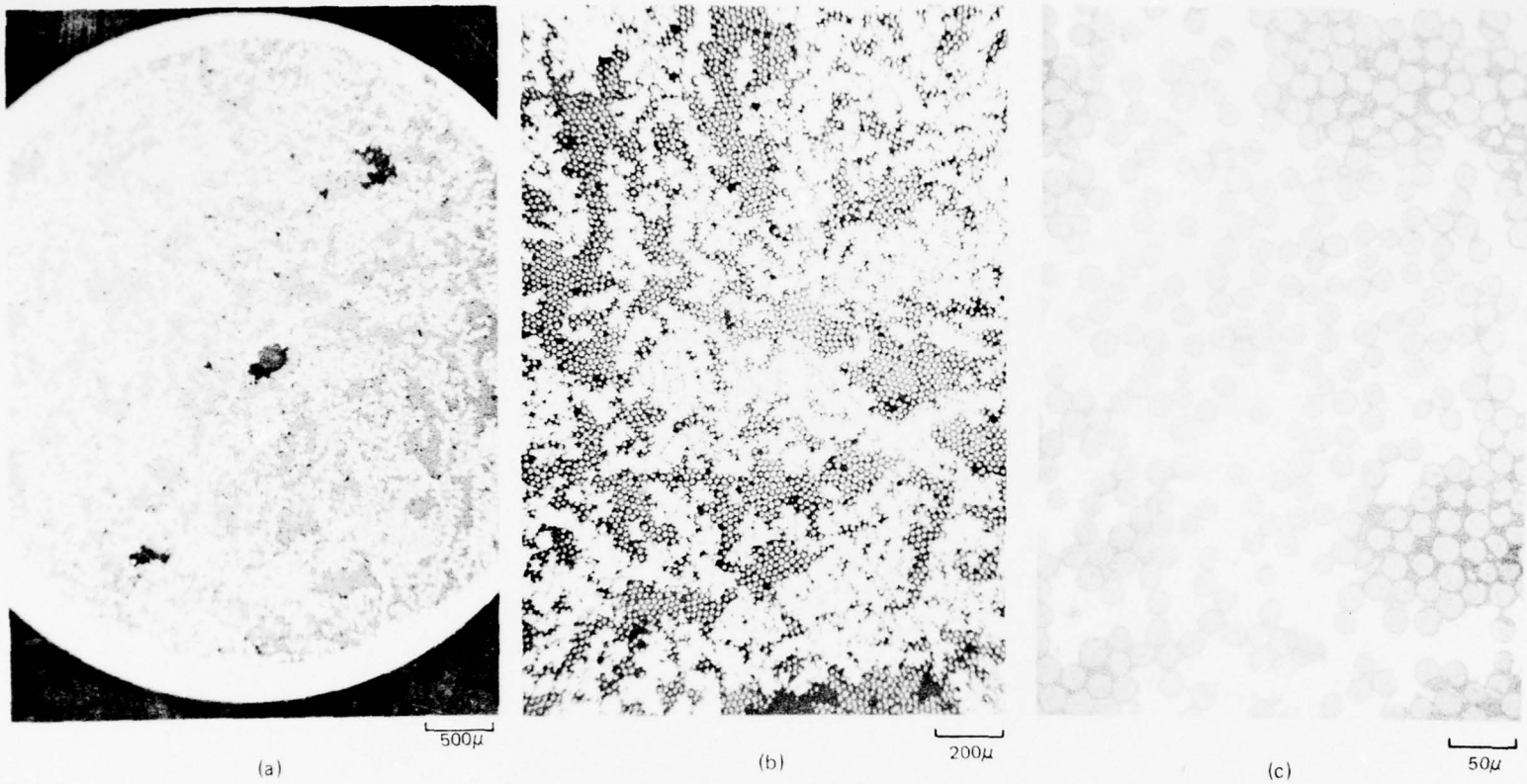

FIG. 22 FP–IV/Al–2% Bi COMPOSITE STRUCTURE (SPECIMEN 9–3)

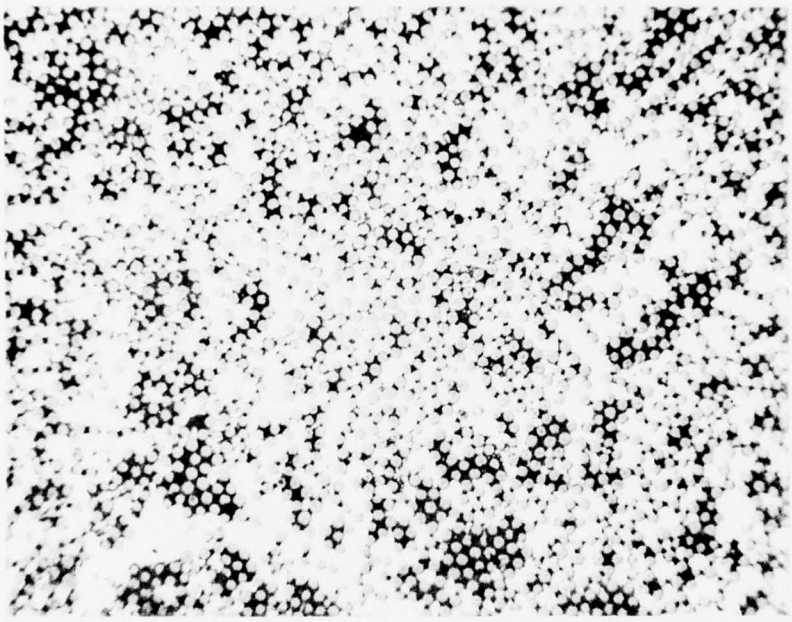

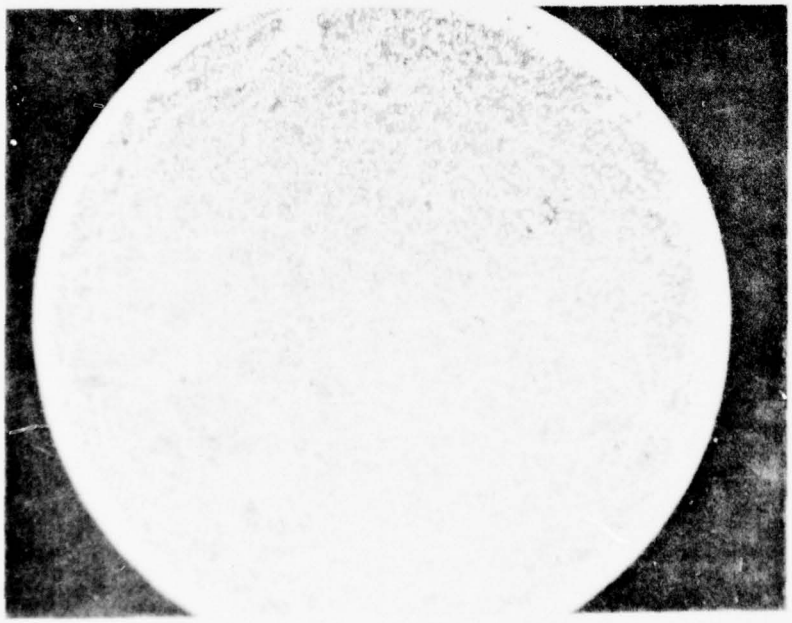

FIG. 23 FP-I/AI-2% Bi COMPOSITE STRUCTURE (SPECIMEN 9-15)

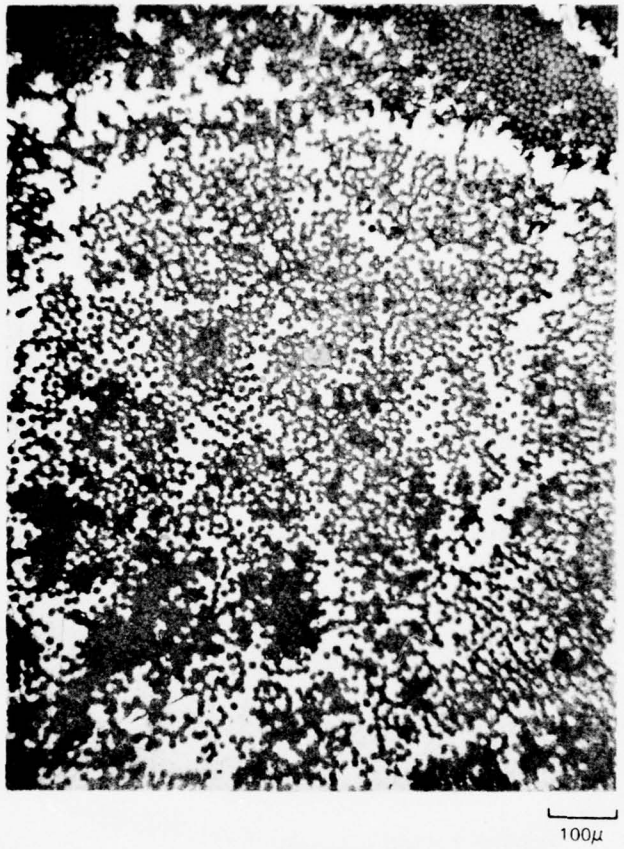

FIG. 24 AB–312/Al–2% Bi COMPOSITE STRUCTURE (SPECIMEN 9–10)

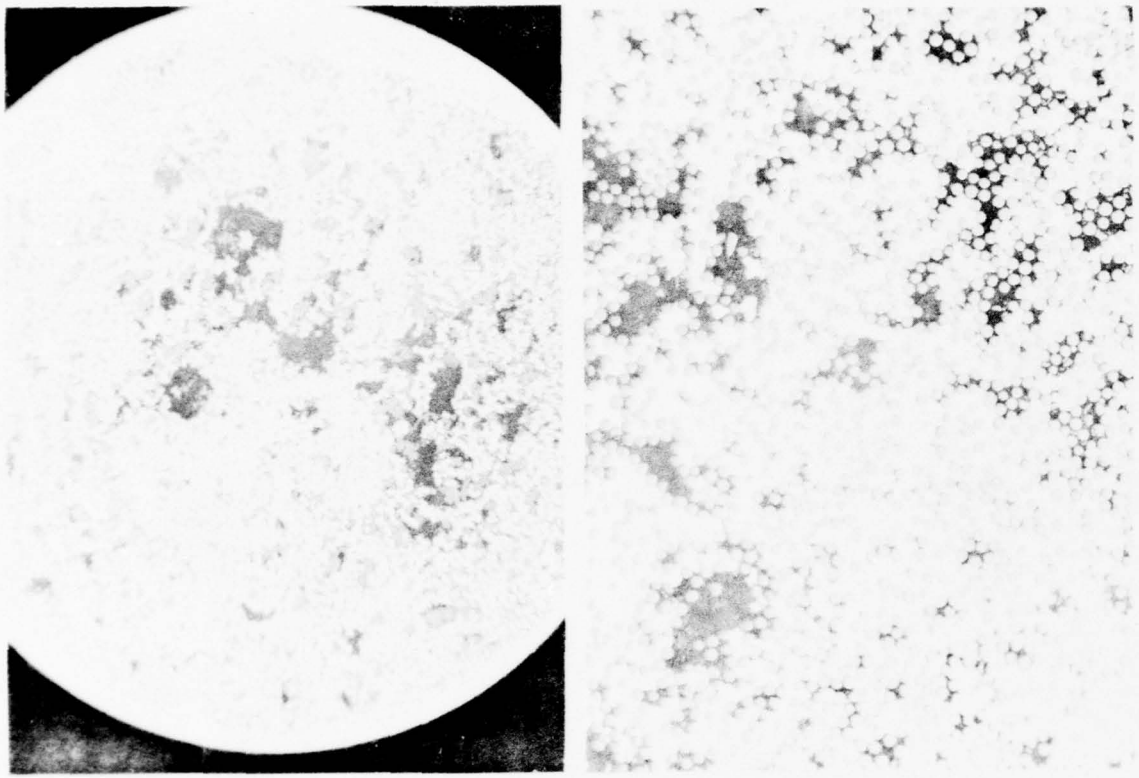

10μ

FIG. 25 FP–IV/Al–10% Mg COMPOSITE STRUCTURE (SPECIMEN 10–4)

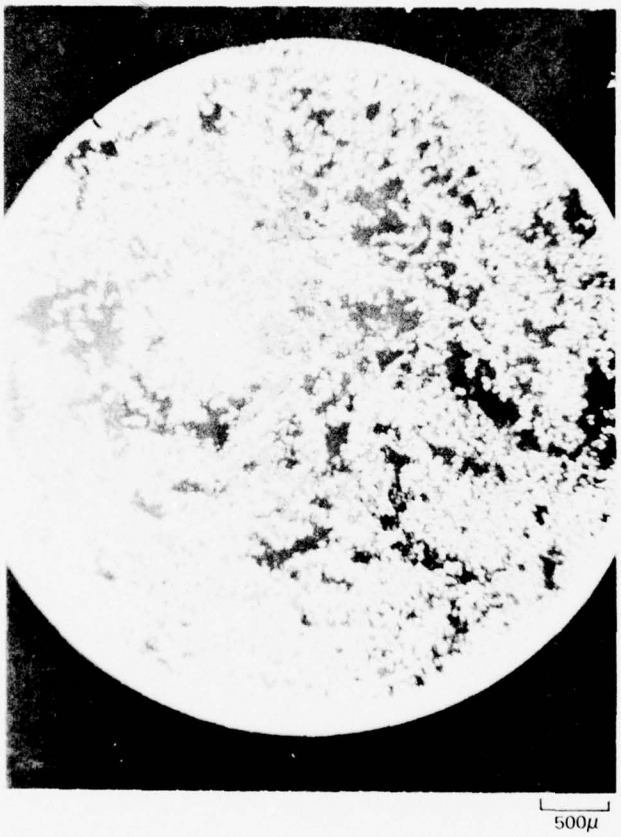

FIG. 26 FP–I/Al–10% Mg. COMPOSITE STRUCTURE (SPECIMEN 10–1)

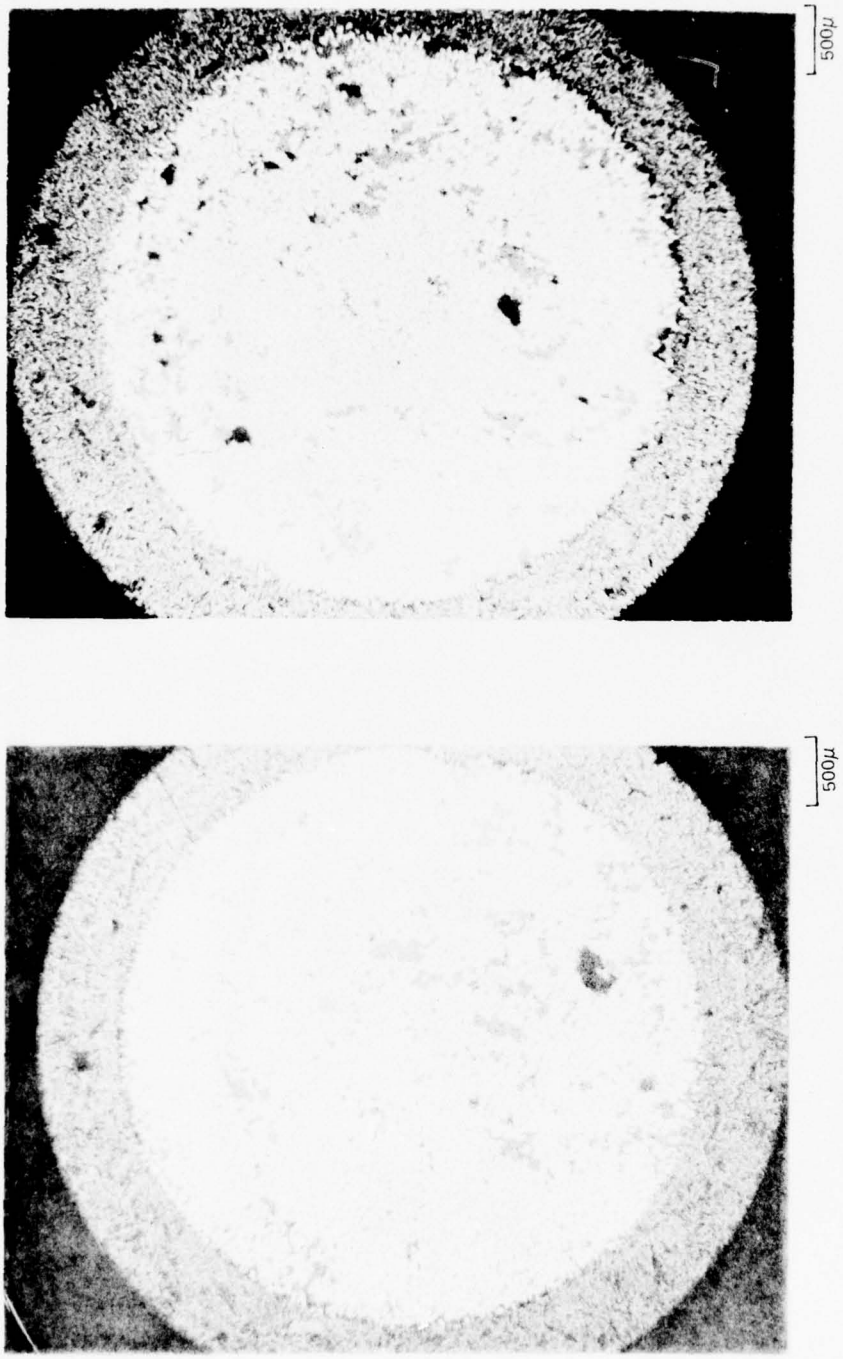

FIG. 27 FP-IV/Al-0.4% Li-10.4% Mg COMPOSITE STRUCTURE (SPECIMEN 16-3)

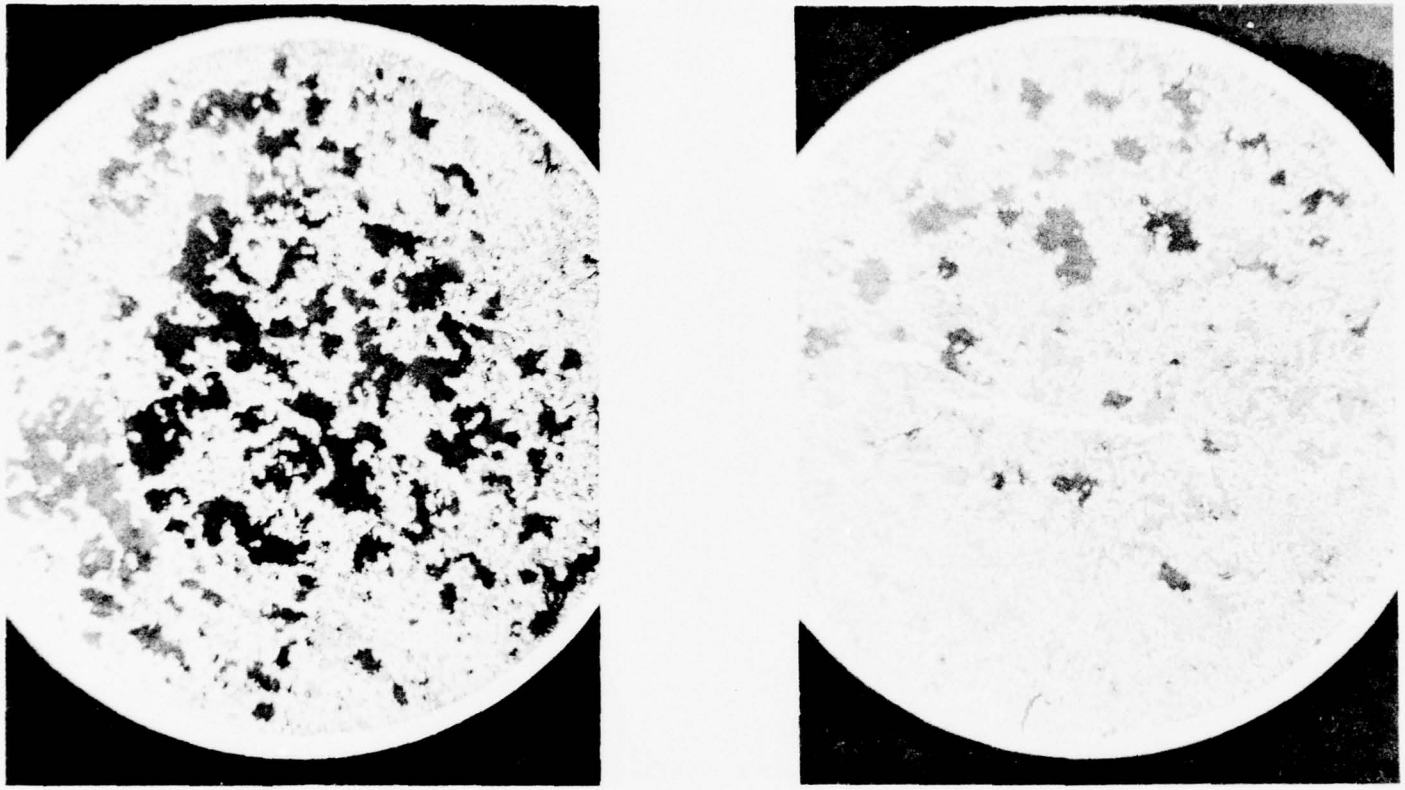

Fig. 28 FP–IV/Al–0.5% Li–5.3% Mg COMPOSITE STRUCTURE (SPECIMEN 15–1)

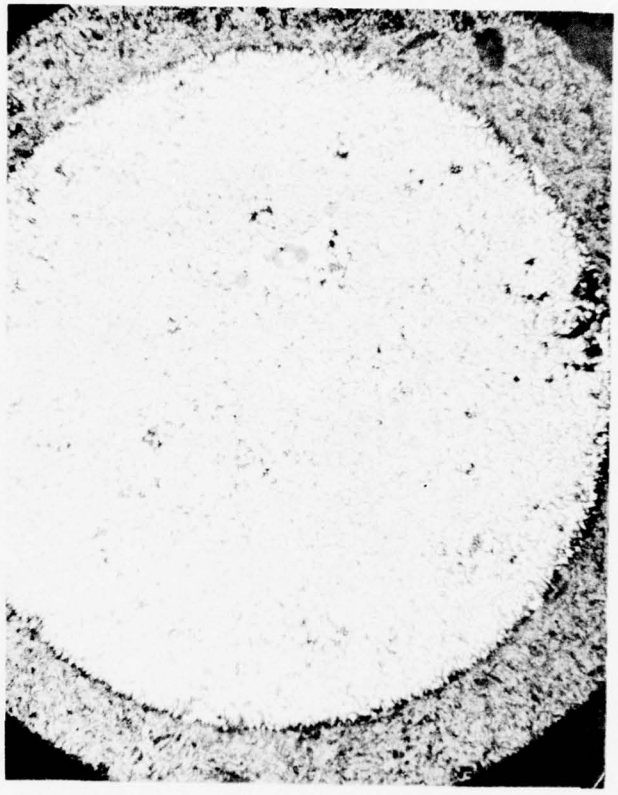

Fig. 29 FP–IV/Al–1.0% Li–11.0% Mg COMPOSITE STRUCTURE (SPECIMEN 13–6)

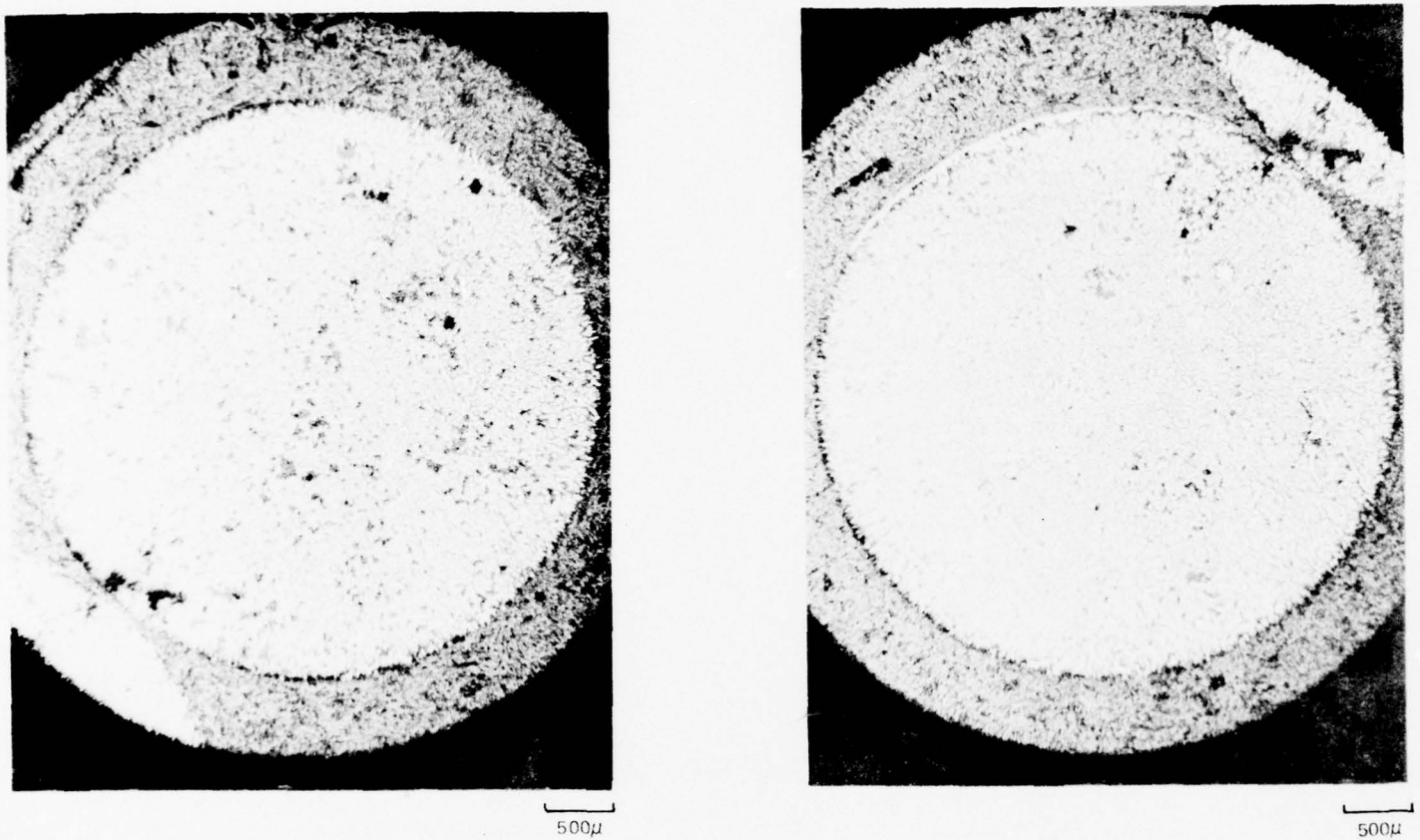

Fig. 30 FP–IV/Al–1.2% Li–3.7 Mg% –0.08 Zr % COMPOSITE STRUCTURE (SPECIMEN 17–5)

Fig. 31 FP-IV/Al-1.2%Li-3.7%Mg-0.08%Zr COMPOSITE WITH INCLUDED ALUMINUM WIRES (SPECIMEN 17-10)

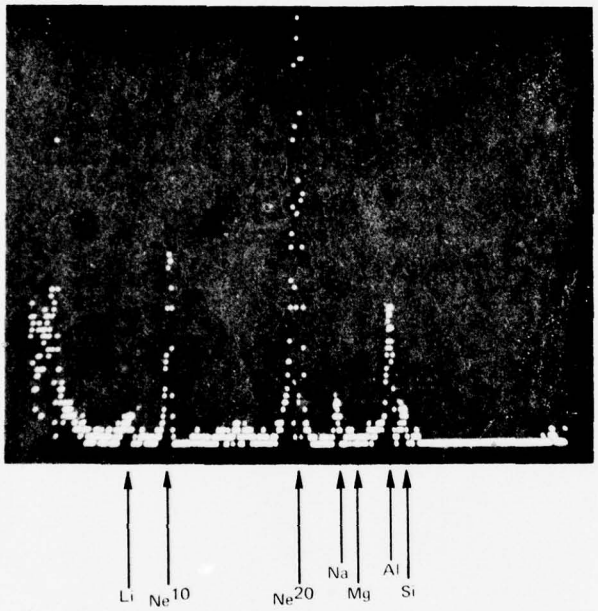

SPECIMEN 9-21
MATRIX = Al-1.37 Bi
PEAK HEIGHT MAG = 4X
SPECTRUM AT 0-5Å
BENEATH SURFACE

FIG. 32 SIMS MASS SPECTRUM FOR EXTRACTED FP-IV FIBERS

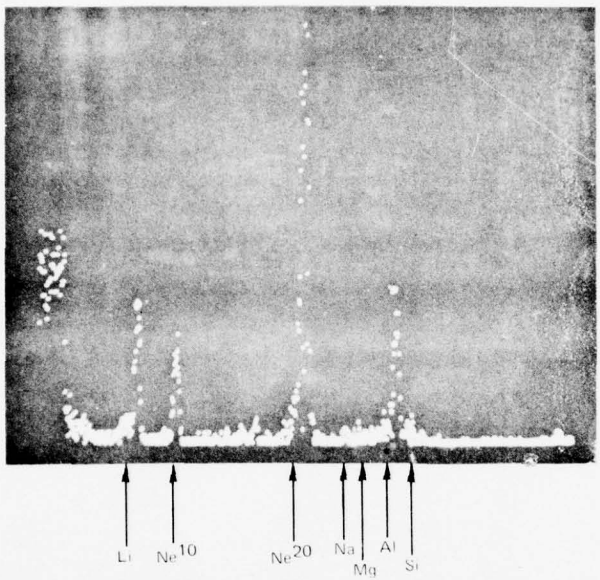

SPECIMEN 15-1
MATRIX = Al-0.5 Li-5.3 Mg
PEAK HEIGHT MAG = 3X
SPECTRUM AT 0-10Å
BENEATH SURFACE

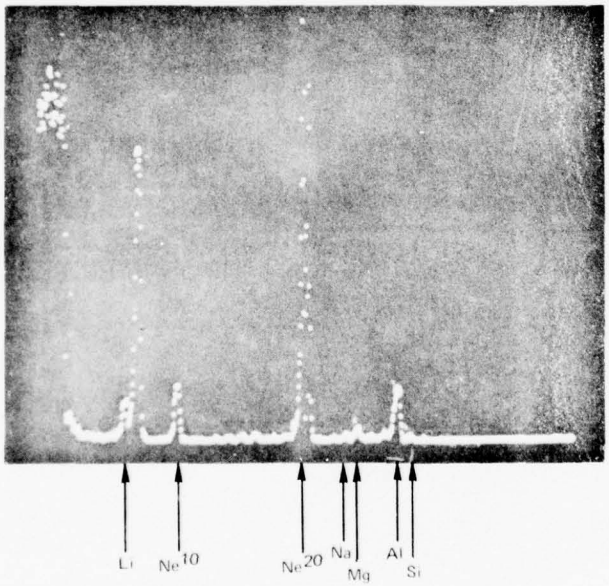

SPECIMEN 18-1
MATRIX Al-1.7 Li-4.0 Mg
PEAK HEIGHT MAG = 2X
SPECTRUM AT 0-5Å
BENEATH SURFACE

FIG. 33 SIMS MASS SPECTRA FOR EXTRACTED FP-IV FIBERS

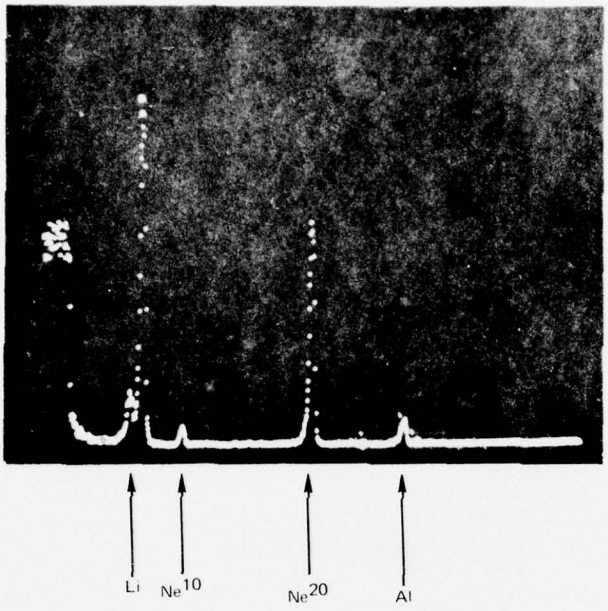

SPECIMEN 6-15
MATRIX = Al-1.71 Li
PEAK HEIGHT MAG = 1X
SPECTRUM AT 0.5-Å
BENEATH SURFACE

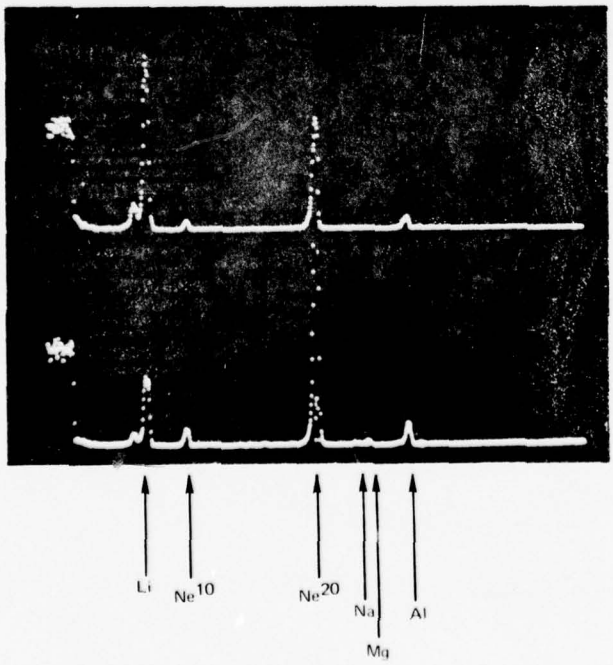

SPECIMEN 6-15
MATRIX = Al-1.71 Li
SPECTRUM AT 0-5Å
BENEATH SURFACE

SPECIMEN 18-1
MATRIX = Al-1.7 Li-4.0 Mg
SPECTRUM AT 0-5Å
BENEATH SURFACE

FIG. 34 SIMS MASS SPECTRA FOR EXTRACTED FP-IV FIBERS

77-04-251-1

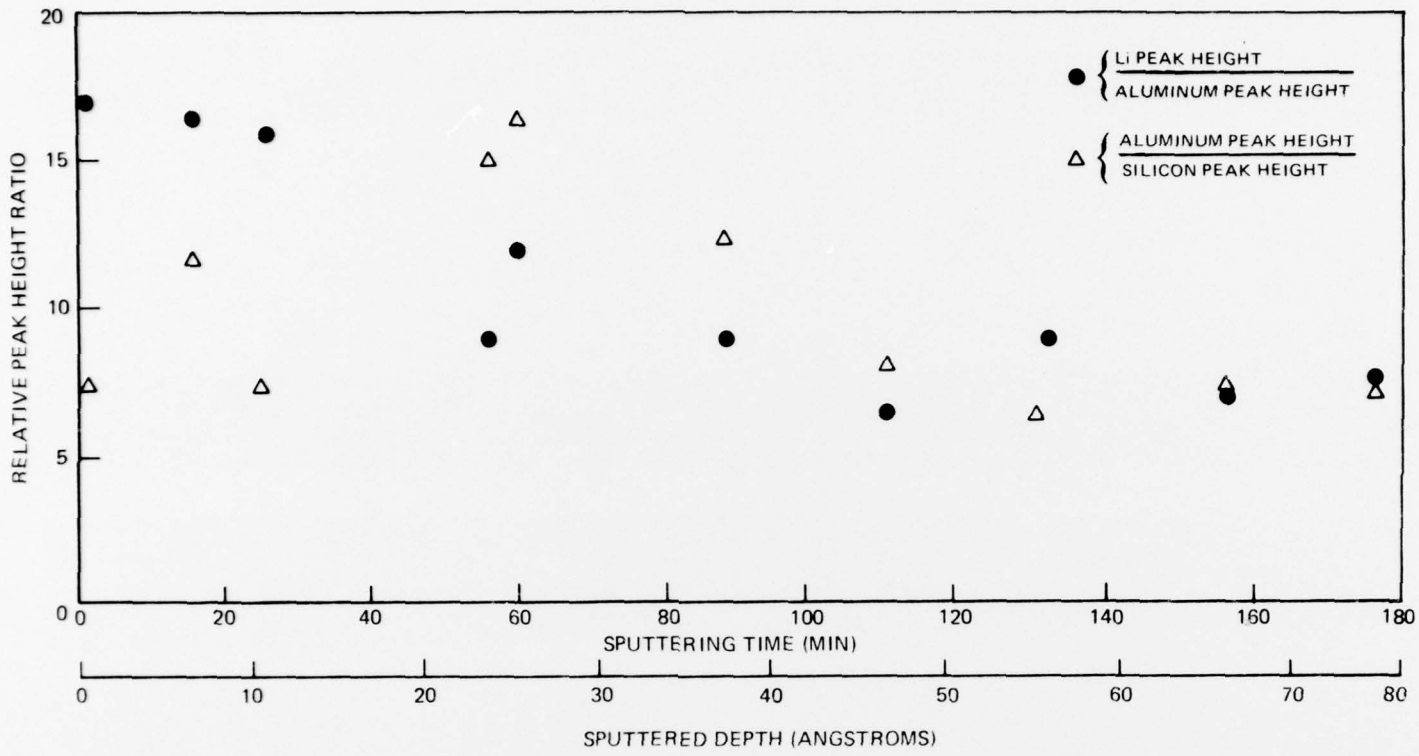

FIG.35 CHANGE IN SIMS SPECTRUM RELATIVE PEAK HEIGHTS FOR FP--IV FIBERS EXTRACTED FROM COMPOSITE 6–15

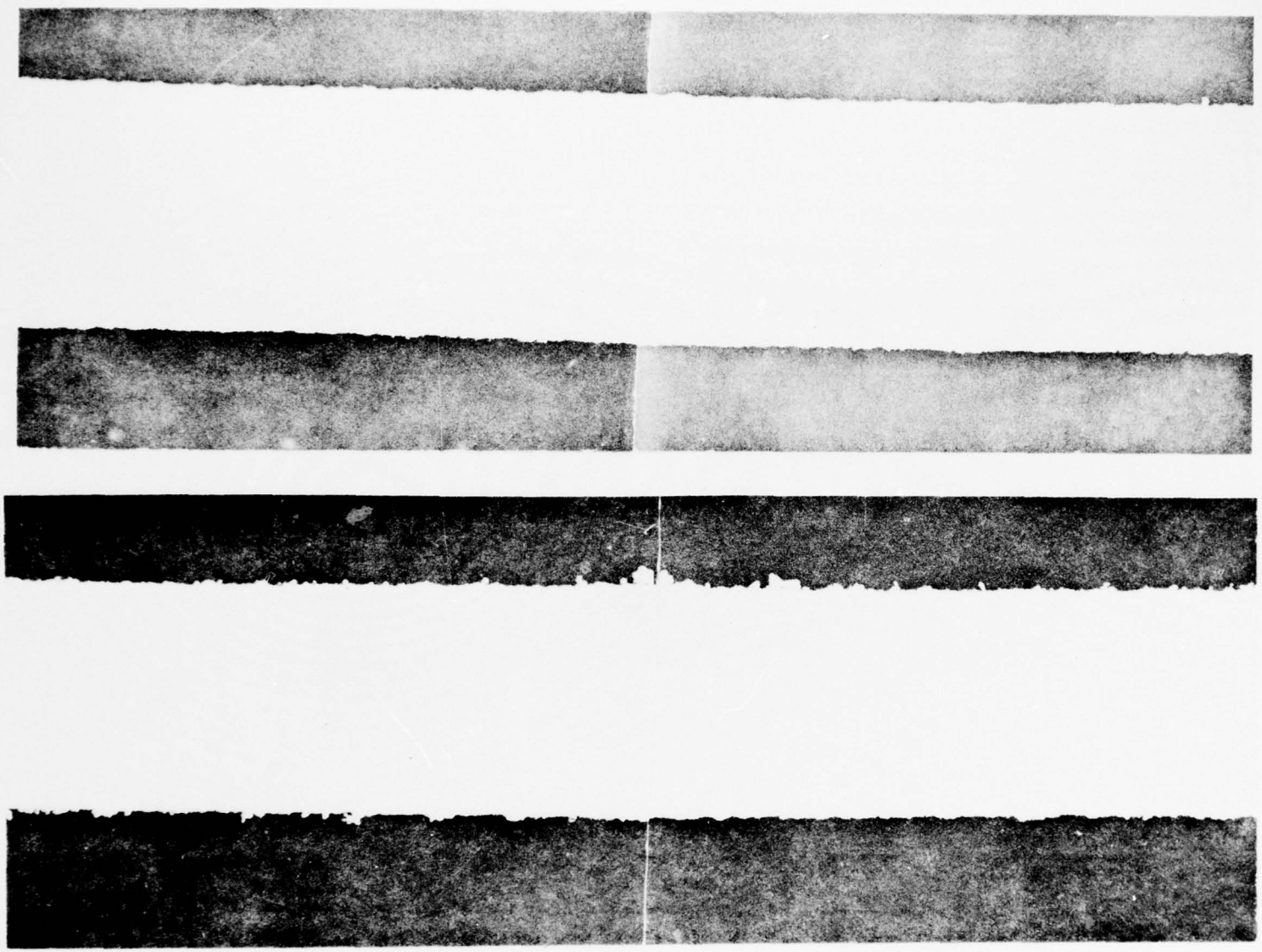

55 μ

FIG. 36 ELECTRON MICROGRAPHS OF TYPICAL LENGTHS OF AS-RECEIVED (UPPER) AND CHEMICALLY EXTRACTED (LOWER) FP-IV FIBERS

1μ

FIG. 37 PROFILE VIEW OF FP–IV FIBER EXTRACTED FROM Al–Li ALLOY MATRIX AND ELECTRON DIFFRACTION PATTERN OBTAINED FROM FIBER SURFACE. MATERIAL PROTRUDING FROM SURFACE IDENTIFIED AS LITHIUM SPINEL

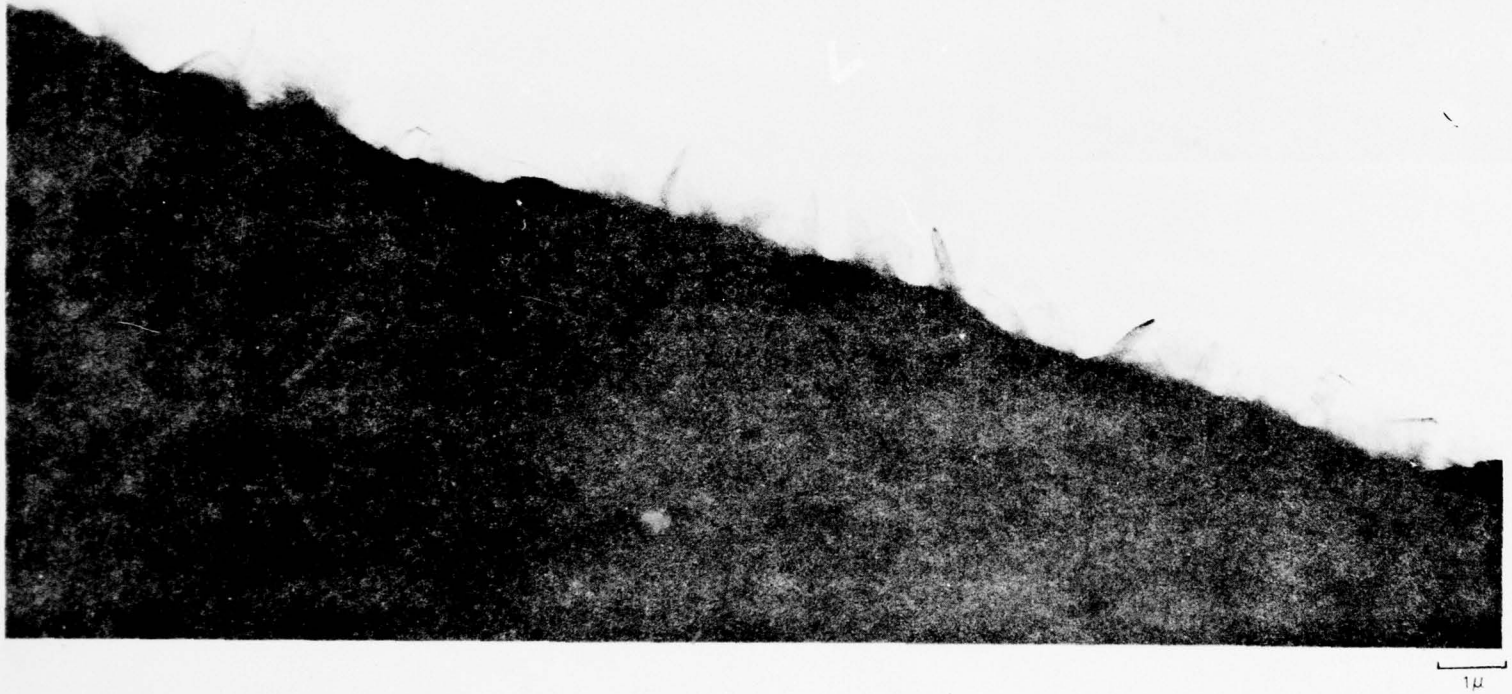

FIG. 38 PROFILE VIEW OF FP–IV FIBER EXTRACTED FROM Al–Li ALLOY MATRIX AND ELECTRON DIFFRACTION PATTERN OBTAINED FROM SMALL SINGLE CRYSTAL PLATELETS WHICH WERE A MINOR (5%) SURFACE CONSTITUENT

SEM ANGLE = 0° 500 μ

SEM ANGLE = 30° 500 μ

Fig. 39 FRACTURE SURFACE OF SPECIMEN 19-26
50 % FP-IV/Al-2%Li
UTS-584 MPa (84.6Ksi)

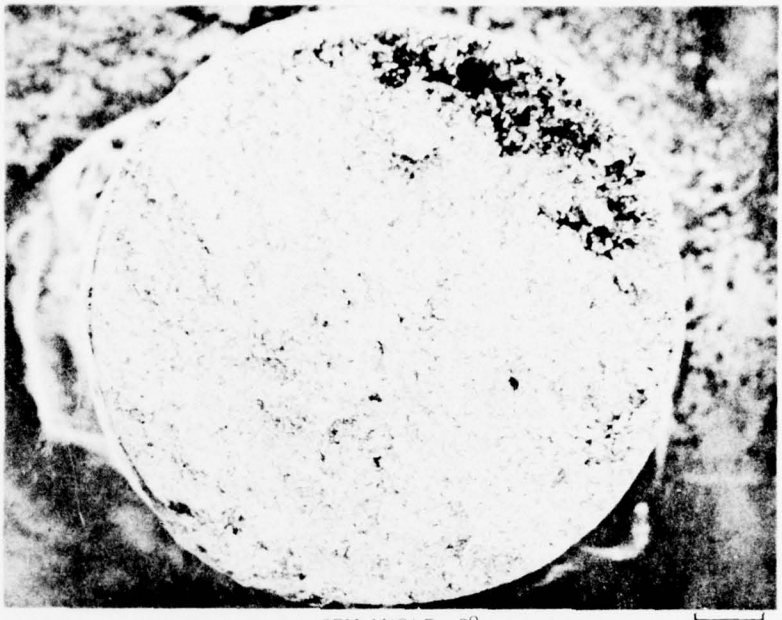

Fig. 40 FRACTURE SURFACE OF SPECIMEN 19–10
34% FP–IV/Al-2%Li
UTS=349 MPa(50.6 Ksi)

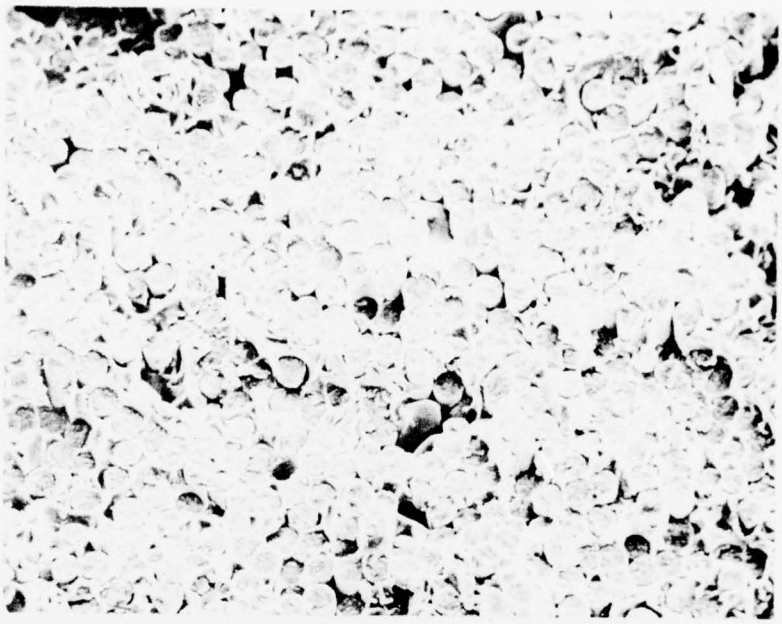

SEM ANGLE = 30°

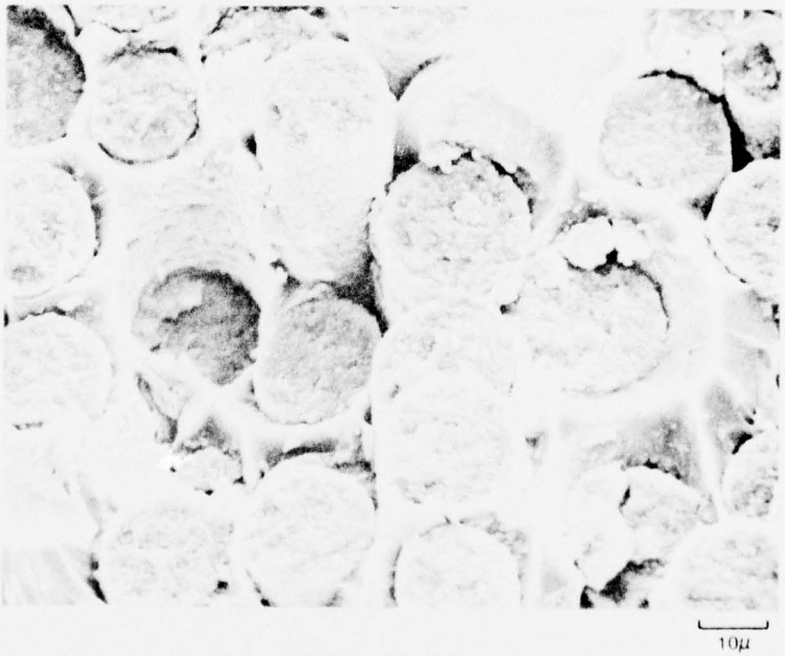

SEM ANGLE = 30°

Fig. 41 FRACTURE SURFACE OF SPECIMEN 19-26

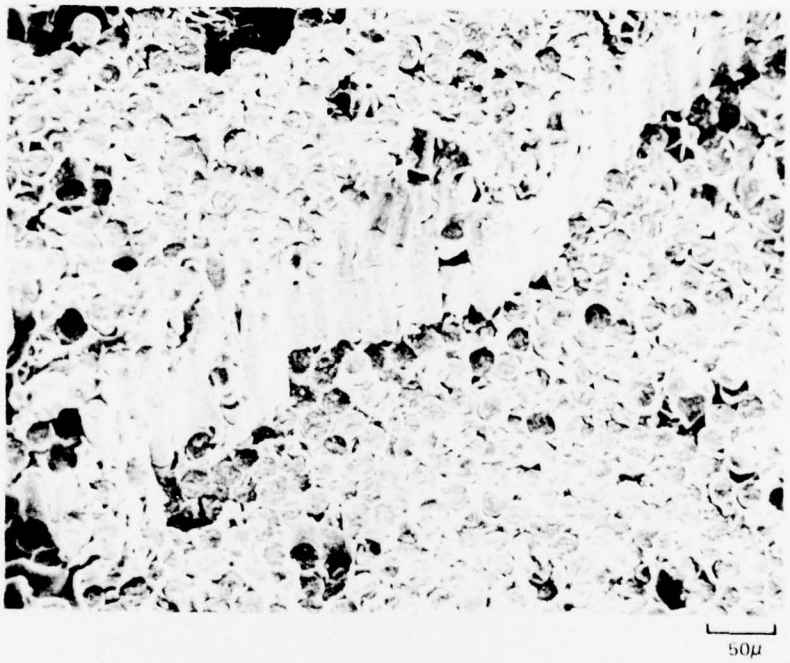

Fig. 42 FRACTURE SURFACE OF SPECIMEN 19-26

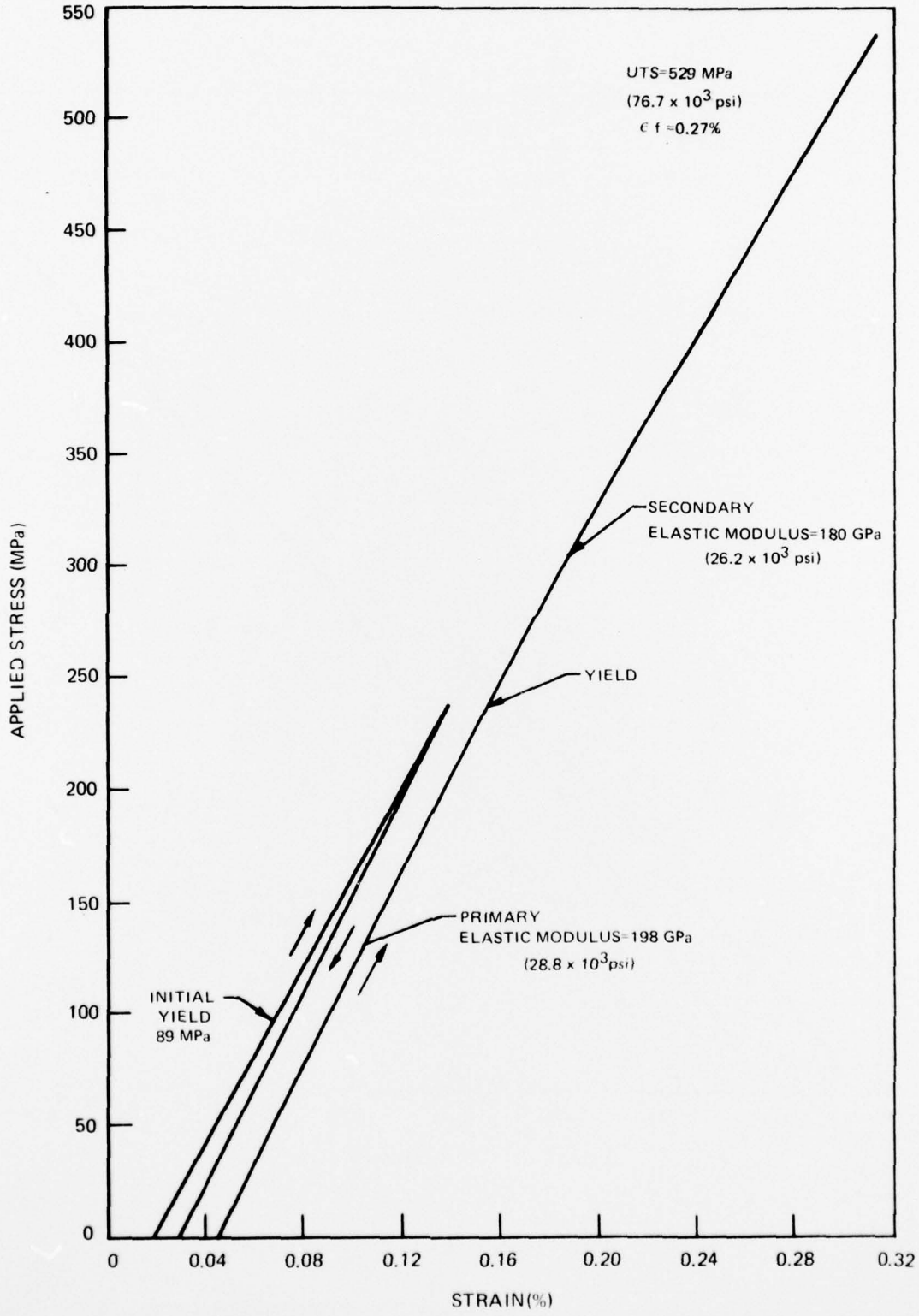

FIG.43 TENSILE STRESS STRAIN CURVE FOR SPECIMEN 19-28 50 % FP FIBER IN ALUMINUM

77-04-251-24

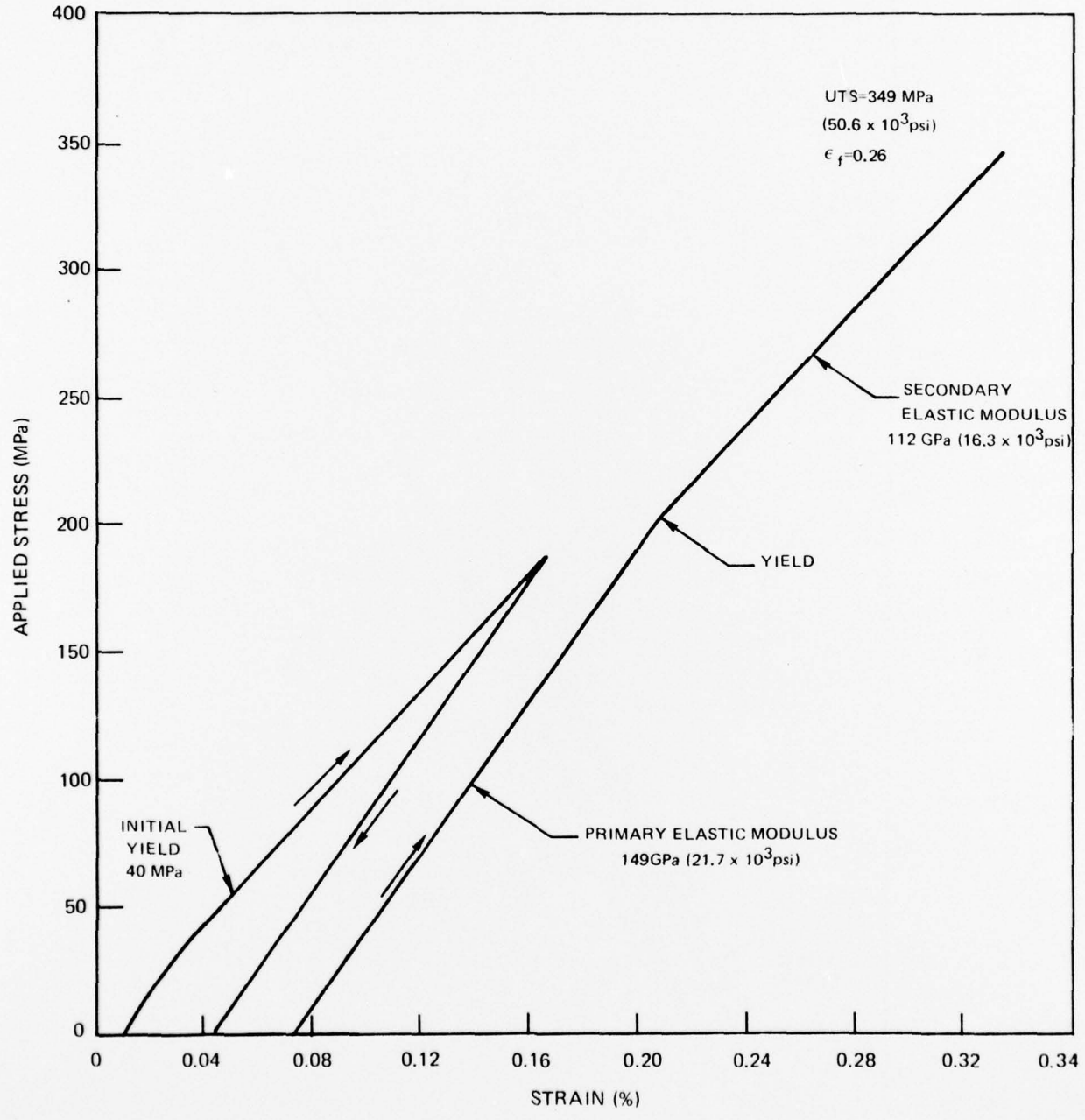

FIG.44 TENSILE STRESS STRAIN CURVE FOR SPECIMEN 19–10
34 % FP FIBER IN ALUMINUM

SEM ANGLE 45°

SEM ANGLE 30°

Fig. 45 FRACTURE SURFACE OF SPECIMEN 2-12
55% FP-IV/Al - 3.3%Li
UTS=4 85 MPa(70.5 Ksi)

R77-912245-3

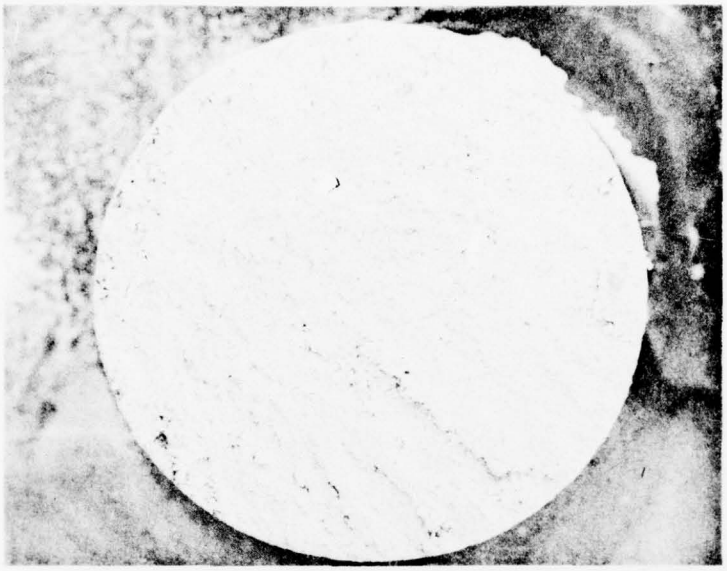

SEM ANGLE = 0

1000 μ

SEM ANGLE 30°

1000μ

Fig. 46 FRACTURE SURFACE OF SPECIMEN 18-1
55% FP-IV/Al-1.7%Li-4.0%Mg
UTS=571MPa(82.8Ksi)

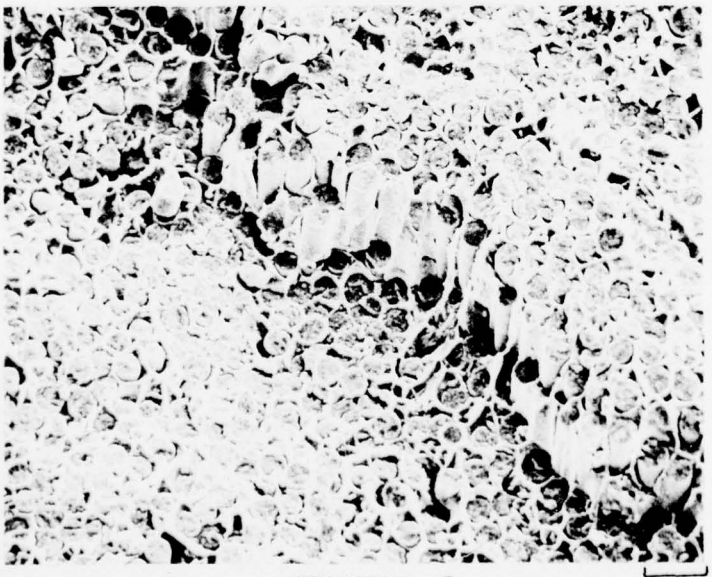

Fig. 47 FRACTURE SURFACE OF SPECIMEN 18-1

FIG. 34 SIMS MASS SPECTRA FOR EXTRACTED FP–IV FIBERS

77-04-251-1

R77-912245-3

SEM ANGLE = 0°

500 μ

SEM ANGLE = 30°

500 μ

Fig. 48 FRACTURE SURFACE OF SPECIMEN 14–2
55% FP–IV/Al–1.1%Li–5.8%Mg
UTS=515 MPa(74.7 Ksi)

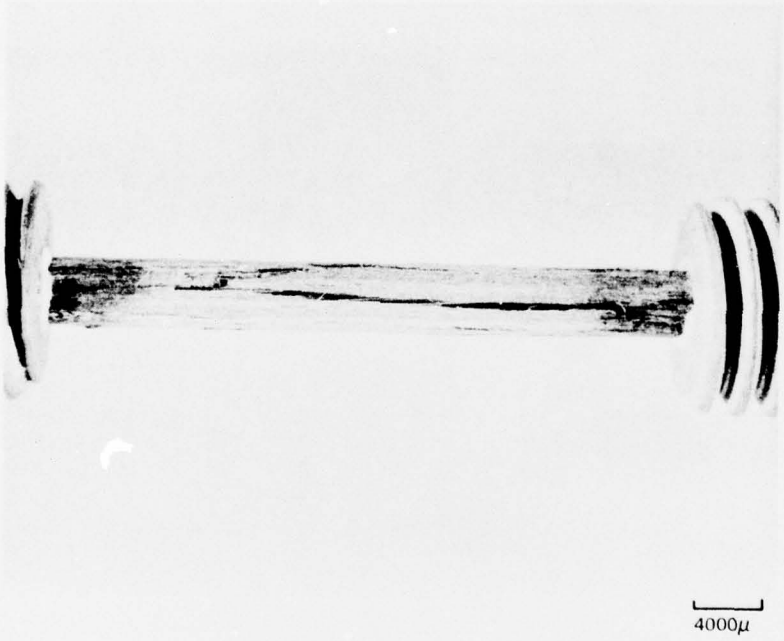

Fig. 49 TENSILE SPECIMEN 9-20
58% FP-IV/Al-1.4% Bi
SPECIMEN STRESSED TO 308 MPa (44.6 Ksi)